HAL
open science

Nose-only inhalations of high-dose alumina nanoparticles/hydrogen chloride gas mixtures induce strong pulmonary pro-inflammatory response: a pilot study

Alexandra Bourgois, Dominique Saurat, Suzanne de Araujo, Alexandre Boyard, Nathalie Guitard, Sylvie Renault, Francisca Fargeau, Christine Frederic, Emmanuel Peyret, Emmanuel Flahaut, et al.

To cite this version:

Alexandra Bourgois, Dominique Saurat, Suzanne de Araujo, Alexandre Boyard, Nathalie Guitard, et al.. Nose-only inhalations of high-dose alumina nanoparticles/hydrogen chloride gas mixtures induce strong pulmonary pro-inflammatory response: a pilot study. Inhalation Toxicology, 2021, 33 (9-14), pp.308-324. 10.1080/08958378.2021.1996492 . hal-03427407

HAL Id: hal-03427407

https://hal.science/hal-03427407v1

Submitted on 13 Nov 2021

HAL is a multi-disciplinary open access archive for the deposit and dissemination of scientific research documents, whether they are published or not. The documents may come from teaching and research institutions in France or abroad, or from public or private research centers.

L'archive ouverte pluridisciplinaire **HAL**, est destinée au dépôt et à la diffusion de documents scientifiques de niveau recherche, publiés ou non, émanant des établissements d'enseignement et de recherche français ou étrangers, des laboratoires publics ou privés.

Inhalation Toxicology
International Forum for Respiratory Research

ISSN: (Print) (Online) Journal homepage: https://www.tandfonline.com/loi/iiht20

Nose-only inhalations of high-dose alumina nanoparticles/hydrogen chloride gas mixtures induce strong pulmonary pro-inflammatory response: a pilot study

Alexandra Bourgois, Dominique Saurat, Suzanne De Araujo, Alexandre Boyard, Nathalie Guitard, Sylvie Renault, Francisca Fargeau, Christine Frederic, Emmanuel Peyret, Emmanuel Flahaut, Aurélie Servonnet, Anne-Laure Favier, Ghislaine Lacroix, Sabine François & Samir Dekali

To cite this article: Alexandra Bourgois, Dominique Saurat, Suzanne De Araujo, Alexandre Boyard, Nathalie Guitard, Sylvie Renault, Francisca Fargeau, Christine Frederic, Emmanuel Peyret, Emmanuel Flahaut, Aurélie Servonnet, Anne-Laure Favier, Ghislaine Lacroix, Sabine François & Samir Dekali (2021): Nose-only inhalations of high-dose alumina nanoparticles/hydrogen chloride gas mixtures induce strong pulmonary pro-inflammatory response: a pilot study, Inhalation Toxicology, DOI: 10.1080/08958378.2021.1996492

To link to this article: https://doi.org/10.1080/08958378.2021.1996492

© 2021 The Author(s). Published by Informa UK Limited, trading as Taylor & Francis Group.

Published online: 12 Nov 2021.

Submit your article to this journal

View related articles

View Crossmark data

Full Terms & Conditions of access and use can be found at
https://www.tandfonline.com/action/journalInformation?journalCode=iiht20

INHALATION TOXICOLOGY
https://doi.org/10.1080/08958378.2021.1996492

Taylor & Francis
Taylor & Francis Group

RESEARCH ARTICLE

OPEN ACCESS Check for updates

Nose-only inhalations of high-dose alumina nanoparticles/hydrogen chloride gas mixtures induce strong pulmonary pro-inflammatory response: a pilot study

Alexandra Bourgois[a], Dominique Saurat[a], Suzanne De Araujo[a], Alexandre Boyard[a], Nathalie Guitard[b], Sylvie Renault[c], Francisca Fargeau[c], Christine Frederic[c], Emmanuel Peyret[d], Emmanuel Flahaut[e], Aurélie Servonnet[c], Anne-Laure Favier[c], Ghislaine Lacroix[d], Sabine François[b] and Samir Dekali[a]

[a]Département EBR, Unité Risques Technologiques Emergents, Institut de Recherche Biomédicale des Armées (IRBA), Brétigny-sur-Orge Cedex, France; [b]Département EBR, Unité Radiobiologie, Institut de Recherche Biomédicale des Armées (IRBA), Brétigny-sur-Orge Cedex, France; [c]Département Plateformes et Recherche Technologique, Institut de Recherche Biomédicale des Armées (IRBA), Brétigny-sur-Orge Cedex, France; [d]Unité de toxicologie expérimentale, Institut National de l'Environnement Industriel et des RISques (INERIS), Verneuil-en-Halatte, France; [e]CIRIMAT, Université de Toulouse, CNRS, INPT, UPS, UMR CNRS-UPS-INP No. 5085, Université Toulouse 3 Paul Sabatier, Toulouse cedex 9, France

ABSTRACT

Objective: Solid composite propellants combustion, in aerospace and defense fields, can lead to complex aerosols emission containing high concentrations of alumina nanoparticles (Al_2O_3 NPs) and hydrogen chloride gas (HCl_g). Exposure to these mixtures by inhalation is thus possible but literature data toward their pulmonary toxicity are missing. To specify hazards resulting from these combustion aerosols, a pilot study was implemented.

Materials and methods: Male Wistar rats were nose-only exposed to Al_2O_3 NPs (primary size 13 nm, 10 g/L suspension leading to 20.0–22.1 mg/m^3 aerosol) and/or to HCl_g aerosols (5 ppm target concentration) following two exposure scenarios (single exposures (SE) or repeated exposures (RE)). Bronchoalveolar lavage fluids (BALF) content and lungs histopathology were analyzed 24 h after exposures.

Results: Repeated co-exposures increased total proteins and LDH concentrations in BALF indicating alveolar–capillary barrier permeabilization and cytolysis. Early pulmonary inflammation was induced after RE to Al_2O_3 NPs ± HCl_g resulting in PMN, TNF-α, IL-1β, and GRO/KC increases in BALF. Both exposure scenarios resulted in pulmonary histopathological lesions (vascular congestions, bronchial pre-exfoliations, vascular and interalveolar septum edemas). Lung oxidative damages were observed *in situ* following SE.

Conclusion: Observed biological effects are dependent on both aerosol content and exposure scenario. Results showed an important pro-inflammatory effect of Al_2O_3 NPs/HCl_g mixtures on the lungs of rat 24 h after exposure. This pilot study raises concerns toward potential long-term pulmonary toxicity of combustion aerosols and highlights the importance for further studies to be led in order to define dose limitations and exposure thresholds for risk management at the work place.

ARTICLE HISTORY
Received 8 April 2021
Accepted 6 October 2021

KEYWORDS
Pulmonary inflammation; nose-only inhalation; combustion aerosols; alumina nanoparticles; hydrogen chloride

Introduction

Combustion reactions from different sources can produce high volumes of complex aerosols containing various components as gases and particles in the environment (Sgro et al. 2012; Chivas-Joly et al. 2016). Solid composite propellants use in aerospace and defense fields lead to emission of complex combustion aerosols containing notably alumina (Al_2O_3) particles and hydrogen chloride gas (HCl_g) (Pellett et al. 1983; Meda et al. 2005). Indeed, high concentrations of Al_2O_3 particles and HCl_g were measured close to these propulsion systems under normal use conditions (classified data). Thermochemical simulations based on highly aluminized solid composite propellant (68% ammonium perchlorate and 20% aluminum) also confirm production of high quantities of Al_2O_3 particles and HCl_g during the combustion process (data not shown). Moreover, these pollutants can also be emitted, respectively, by industrial activities such as aluminum manufacturing (Pichard et al. 2005) and wastes incineration (Wang et al. 1999) increasing the risk of exposure to the workers.

Alumina (Al_2O_3) is the oxidized form of aluminum and exists under several crystalline phases (γ, δ, θ, and α) (Piriyawong et al. 2012). Among them, a majority of γ then δ polymorphs were found following solid composite propellants use (Galfetti et al. 2004; Meda et al. 2005). Alumina is

CONTACT Samir Dekali samir.dekali@gmail.com Département EBR, Unité Risques Technologiques Emergents, Institut de Recherche Biomédicale des Armées (IRBA), Brétigny-sur-Orge Cedex, France

Supplemental data for this article can be accessed here.

© 2021 The Author(s). Published by Informa UK Limited, trading as Taylor & Francis Group.
This is an Open Access article distributed under the terms of the Creative Commons Attribution-NonCommercial-NoDerivatives License (http://creativecommons.org/licenses/by-nc-nd/4.0/), which permits non-commercial re-use, distribution, and reproduction in any medium, provided the original work is properly cited, and is not altered, transformed, or built upon in any way.

mainly used for aluminum production and enters in the composition of many everyday products (paper, plastics, ceramics, flame retardants, and coatings) due to its hardness. Otherwise, alumina can also be found in foods and cosmetics (Krewski et al. 2007). To determine health hazard related to alumina particles exposure, only few studies were conducted *in vivo* by inhalation. Twenty-eight days nose-only inhalation of Al_2O_3 NPs (11.94 nm, 0.2–5 mg/m^3, 5 days a week) showed pulmonary pro-inflammatory properties of Al_2O_3 NPs on rats. This was characterized by total cells, polymorphonuclear neutrophils (PMN), lymphocytes, lactate dehydrogenase (LDH), TNF-α, and IL-6 increases in bronchoalveolar lavage fluids (BALF). Alveolar macrophages accumulation was also observed in lungs after 28 days exposure (Kim et al. 2018). In mice, pulmonary pro-inflammatory effects were also recorded after 7 days exposure to 40 nm Al_2O_3 NPs (0.4 mg/m^3) by inhalation. Increased concentrations of IL-6 and IL-33 were measured in BALF associated with emphysema and airway remodeling appearance. However, in this study, BALF PMN concentration was not increased following Al_2O_3 NPs inhalation (Li et al. 2017). Al_2O_3 NPs intratracheal (IT) instillation on rats (6.3 nm, 0.5–300 cm^2/mL) also induced acute pulmonary inflammation resulting in PMN concentration increases in BALF (Cho et al. 2012). Moreover, mice IT instillation exposures to Al_2O_3 particles (4.37 µm, 40 mg) increased macrophages, PMN, and fibronectin concentrations in BALF until 12 months after exposure suggesting pulmonary inflammation persistence over time (Tornling et al. 1993). Another study, carried out by nasal instillation on rats, highlighted dose-dependent inflammation and alveolar–capillary barrier permeabilization after Al_2O_3 particles (size unknown, 1–40 mg/kg) exposure (Kwon et al. 2013). Besides pro-inflammatory properties, several *in vitro* Al_2O_3 particles toxicity studies' results suggest oxidative stress induction and genotoxic potential (DNA single- and double-strand breaks induction) of these particles (Sliwinska et al. 2015; Zhang et al. 2017). These effects were also found *in vivo* after oral, intravenous, or peritoneal injection exposures to Al_2O_3 particles (Chen et al. 2008; Balasubramanyam et al. 2009; Prabhakar et al. 2012; Zhang et al. 2017). Furthermore, aluminum is a known respiratory sensitizer which can induce immune response resulting in allergies and occupational asthma (Cohen 2004; Zhu et al. 2013; Kongerud and Soyseth 2014).

Hydrogen chloride gas is a known irritant and caustic agent able to cause severe ocular and cutaneous lesions (Dyer and Esch 1976). In water, HCl_g dissolves to form hydrochloric acid solution (HCl). HCl_g and HCl exposure risk is non-negligible as these compounds are widely used in industries and laboratories and as they can be found in some household products (Dawe et al. 2019). After HCl_g inhalation by rats and mice, eyes, mucous membranes, and skin irritations were observed which is associated with respiratory system lesions (emphysema, atelectasis, and edema) (Darmer et al. 1974). Respiratory system necrosis as well as PMN increases were also observed on rats after 30 min inhalation (1284 and 1293 ppm of HCl_g) (Stavert et al. 1991). Nevertheless, HCl_g long-term inhalation (10 ppm; 6 h a day 5 days a week) performed during rats entire life did not induce neoplastic or preneoplastic lesions (Sellakumar et al. 1985). Similar respiratory symptoms were found in Guinea pigs and rabbits associated with severe and persistent inflammatory reactions (Machle et al. 1942). Mitogenic effect of HCl (40 mM) was also shown on rabbit esophageal mucosa after 1 h incubation (Carpizo et al. 1998). Moreover, respiratory rate increase and oxygen partial pressure in blood decrease were observed after HCl_g head-only inhalation in baboons (500, 5000, and 10,000 ppm; 15 min). However, no alteration of pulmonary function was reported 3 months post-exposure (Kaplan et al. 1988). Pro-inflammatory effect of HCl was also demonstrated *in vitro* on esophageal mucosa and mice macrophages (cell line RAW 264.7), resulting in an increase in the substance P, IL-8, IL-6, IL-1β, platelet-activating factor (PAF), and nitric acid levels (Kellum et al. 2004; Cheng et al. 2006; Cheng et al. 2006; Ma et al. 2010).

Taken together, these toxicity data regarding Al_2O_3 particles and HCl_g raise questions toward their potential combined toxicity due to possible exposure to the workers. The study of mixtures effects is an actual major concern in toxicology. Only few scientific data are available in literature, especially for mixtures of compounds with different physical forms (solid and gas for example). However, population is daily exposed to multiple pollutants simultaneously and a recent study highlighted mixtures effects (synergy, addition, antagonism, or inhibition) unpredictability (Hayes et al. 2019). Therefore, it is currently necessary to study mixtures effects in a case-by-case basis. Biological effects and resulting hazard of complex combustion aerosols exposure are poorly described in literature. To date, only one study was published concerning the combined effect of Al_2O_3 particles and HCl_g. This study was carried out *in vivo* on rats and mice by whole body exposure (Wohlslagel et al. 1976). However, during exposures, HCl_g was always associated with hydrogen fluoride gas (HF_g) and the only studied endpoint was mortality. Conclusions did not highlight any additive or synergistic effect of Al_2O_3 particles addition to the mixture of gases on animals' mortality.

Due to the lack of scientific data in literature concerning biological effects of mixtures containing NPs and other environmental pollutants, performing *in vitro* and *in vivo* studies is essential to improve knowledge on toxicological impact on human health. Following solid composite propellant combustion, high concentrations of hydrogen chloride gas (HClg) and alumina nanoparticles (Al_2O_3 NPs) are produced. Therefore, our pilot study focused on exposure to mixture of aerosols containing HClg and Al_2O_3 NPs. Inhalation is the main route of exposure to these combustion aerosols, and little is known about combined effects of HClg and Al_2O_3 NPs on the respiratory tract. Consequently, our objective was to assess the early pulmonary effects of model aerosols mimicking an inhalation exposure to combustion aerosols from solid composite propellants on rats. To investigate toxicological effects, animals were nose-only exposed 4 h (single exposures; SE) or 4 h a day for 4 days

(repeated exposures; RE) to aerosols. To assess pro-inflammatory response and oxidative stress induction, BALF content, and lungs histopathology were analyzed 24 h after exposures end.

Material and methods

Test materials

Alumina nanoparticles (Al_2O_3 NPs) were provided by Sigma-Aldrich (St. Louis, MO, USA) (718475) with the following physico-chemical specifications: primary size 13 nm, crystalline phase gamma/delta (γ/δ), specific surface (85–115 m^2/g) experimentally confirmed by the Brunauer, Emmet, and Teller method (BET) (97 m^2/g), pH (4.5–5.5), and purity 99.8%. HCl_g was calibrated, certified, and provided by Air Liquide (0023159805-000010; "Saphir" quality). Initial HCl_g concentration is 500 ppm in the gas cylinder.

Animals

All *in vivo* experiments were approved by the "Comité Régional d'Ethique en Matière d'Expérimentation Animale de Picardie" (CREMEAP, CNREEA registration code: C2EA-96). Healthy 7-week-old male rats WISTAR RjHan:WI, Janvier Labs; 250 g) were housed in polycarbonate cages, at a temperature of 20–24 °C, and a relative humidity of 40–70% controlled room, and had free access to food and water *ad libitum*. A 12 h light–12 h dark cycle was respected. Animals (2–3 rats/cage) were acclimatized for at least 5 days before experiments. Wistar rats were selected for this project as they are often used in inhalation studies (Parasuraman 2011).

Animal exposure

Two exposure scenarios were tested in this study. Single exposures (SE) of 4 h and repeated exposures (RE) of 4 h a day for 4 days were performed. These scenarios were adapted from OECD guidelines 403 "Acute Inhalation Toxicity" and 436 "Acute Inhalation Toxicity – Acute Toxic Class Method" (OECD/OCDE403 2009a; OECD/OCDE436 2009c) recommendations. The 96 animals were distributed in 8 groups of 12 rats (6 rats for biochemistry analysis, 3 rats for histopathology analysis, and 3 rats for aluminum quantification in lungs among each group), respectively, exposed to air (control group, inhaling air mixed with nebulized ultrapure water), HCl_g, Al_2O_3 NPs or Al_2O_3 NPs/HCl_g for each exposure scenario. They were exposed in a nose-only inhalation tower (randomized placement on the inhalation tower) to nebulized Al_2O_3 NPs suspensions in ultrapure water (10 g/L, a high dose to simulate a worst case scenario) using a PALAS AGK 2000E (Palas) and/or to HCl_g (target concentration 5 ppm, French Occupational Exposure Limit (OEL)). For Al_2O_3 NPs, the choice was based on a preliminary study results in which intratracheal instillations of 10 µg of Al_2O_3 NPs did not induce biological effect while instillations of 500 µg of Al_2O_3 NPs led to pro-inflammatory response (data not shown). HCl_g French OEL was selected to conduct this pilot study in the absence of field data related to HCl_g precise concentrations generated by solid composite propellants use. Exposure flow was controlled using regularly checked mass flow meters (TYLAN). Both compounds were mixed (Al_2O_3 NPs/HCl_g exposures) prior to entering into the inhalation tower at a 20 L/min flow rate. Samples were taken on bubblers (two bubblers in series) or cellulose filters using mass flow meters to allow aerosols characterization. A neutralization system (bubblers with caustic soda and desiccant) was placed at the exposure device exit to eliminate generated aerosols (Figure 1). Rats were euthanized by isoflurane inhalation 24 h after the last exposure end and biological samples were collected for further analysis according to the OECD guidelines 412 "28-day (sub-acute) inhalation toxicity study" (OECD/OCDE412 2009b).

Monitoring and characterization of aerosols

To precisely characterize generated aerosols and ensure their stability over time, samples were collected directly from the inhalation tower (empty animal exposure tube location) regularly during exposures (30 min, 2 h and 3h30 after exposure beginning). Aerosols characterization was only performed during rats single 4-h exposures assuming that repeated exposures would result in similar exposures. Al_2O_3 NPs aggregates size, form, and chemical composition were studied. Transmission electron microscopy (TEM) imaging on Al_2O_3 NPs bulk powder was performed using electron microscope JEOL JEM 1400 operated at 120 kV equipped with an CCD camera (Gatan Orius 1000, Gatan Inc., Warrendale, PA, USA). Aerosol samples were collected on copper grids and TEM observations were performed using a CM12 80 kV microscope (Philips, Tokyo, Japan) equipped with a Megaview 3 camera (EMSIS) and an EDX probe. Al_2O_3 NPs crystal structure and size of crystallites were determined by X-ray powder diffraction (XRD) using a D4 ENDEAVOR X-ray diffractometer (Bruker, Karlsruhe, Germany). XRD patterns were acquired with the use of Cu-Kα radiation ($\lambda = 1.5406$ Å) from powders directly hand-pressed on sample holders. Sioutas (SKC Inc., Seoul, South Korea) cascade impactor was used to precise the NPs sizes distribution and concentrations in the aerosols. Sampling was performed during aerosol generation (Al_2O_3 NPs alone or with HCl_g) without animals as it requires a 9 Lpm (liter per minute) flow rate during 15 min. The mean aerodynamic diameter was calculated from Sioutas data using the following formula: aerodynamic diameter (nm) = $\sum$ (mass % x stage size (µm)) × 1000. The stability of Al_2O_3 NPs concentrations during exposures was assessed using inductively coupled plasma optical emission spectrometry (ICP-OES) to quantify aluminum on cellulose filters after samples collection (1 Lpm, 15 min), as recommended by AFNOR standard NF-EN-ISO-11885. Analyses were performed on ICP-OES 5110 (Agilent, San Deigo, CA, USA) with ICP Expert II 7.3 software (Agilent).

HCl_g content was assessed indirectly by chloride ions (Cl^-) dosing on bubbler samples (free fraction, two bubblers

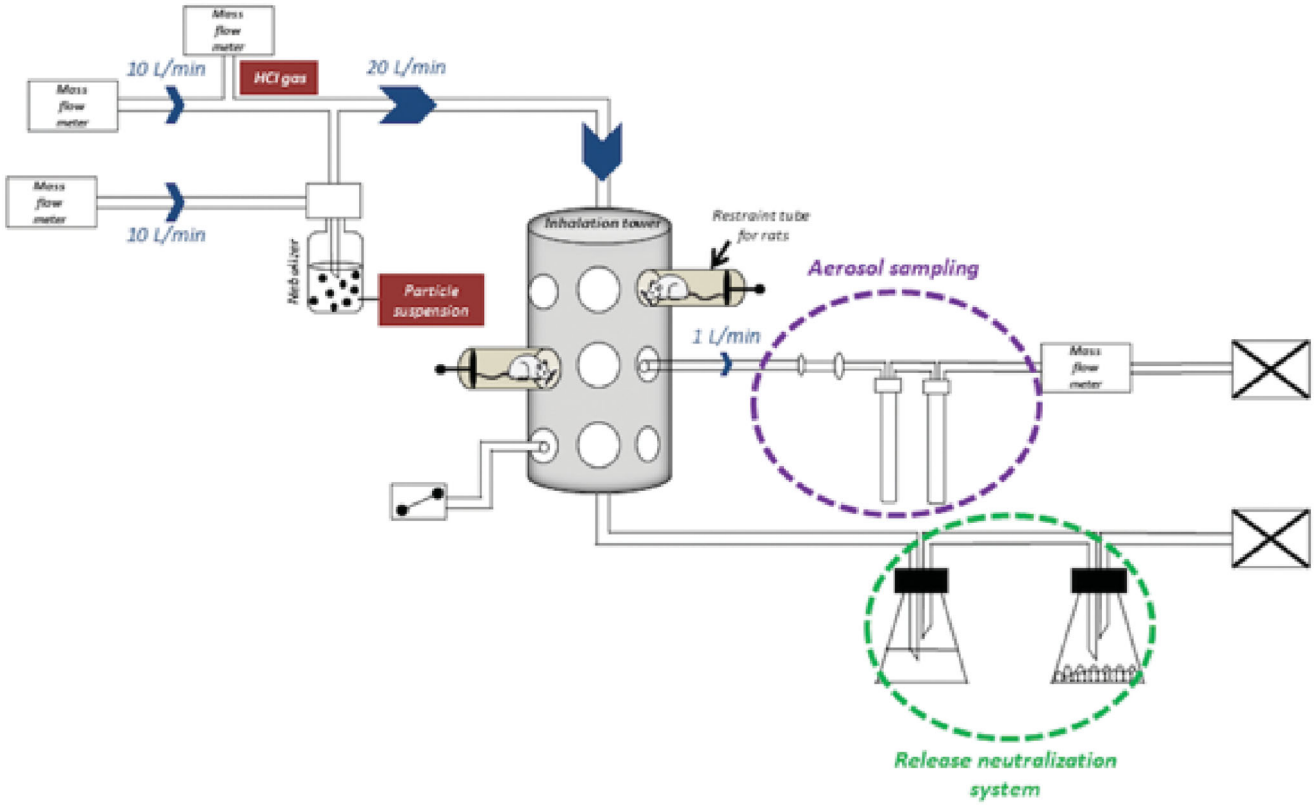

Figure 1. Nose-only inhalation exposure system. Al_2O_3 NPs aggregates suspension in water and HCl_g bottle were connected to the system on two parallel paths that joined to create the mixture. Mass flow meters allowed to generate and calibrate the air flow in order to avoid re-inhalation phenomena of the air exhaled by the animals (dynamic air circulation, 10 L/min). During exposures, rats were placed in individual containment tubes positioned on the oro-nasal inhalation tower. Al_2O_3 NPs and HCl_g mixture reached the inhalation chamber at a flow rate of 20 L/min. Bubblers and samplers connected to the inhalation tower allowed the collection of samples during the exposures in order to characterize the generated aerosol. A release neutralization system (bubbler with soda and desiccant) was set up at the inhalation tower exit.

placed in series) and on cellulose filters (particulate fraction) using ion exchange chromatography according to AFNOR standard NF-EN-1911. The sampling was performed over 15 min at a flow rate of 1 Lpm.

Aluminum quantification in lungs

Rats ($n = 3$) were euthanized 24 h after the last exposure end and perfused with phosphate-buffered saline (PBS) to remove blood from the lungs. Aluminum burden was then quantified using ICP-OES. Briefly, tissue samples were digested in a mixture of concentrated nitric acid (HNO_3; Analpure® Analytika 69% for SE and Normatom VWR 67–69% for RE) and hydrofluoric acid (HF; Analpure® Analytika 48% for SE and Normatom VWR 47–51% for RE) using a microwave oven (Mars Xpress CEM for SE and Ethos One Milestone for RE). After cooling at room temperature, boric acid solution was added to neutralize digests (H_3BO_4; Ultra-pure Chem Lab 99.9% for SE and Suprapur® Merck 99.9999% for RE) and samples were diluted in ultra-pure water (at a final volume of 50 mL). Aluminum quantification was then performed using ICP-OES 5110 (Agilent, for SE, LLOQ[1] = 0.25 µg/g of lung) or ICP-OES Optima 8300 (PerkinElmer, Waltham, MA, USA, for RE, LLOQ = 1.25 µg/g of lung). Software used to realize spectra analysis were ICP Expert II 7.3 (Agilent, for SE) or WinLab32 ICP v5.5 (PerkinElmer, for RE). The equipment and reagents change should not have influenced experimental results as LLOQ were in each case was lower than measured values and as the reagents used had the same quality and concentration.

Clinical symptoms and body weight

Daily monitoring of clinical symptoms was performed throughout the experiment. Respiratory, behavioral, and dermal visible changes were watched. Type, date of occurrence, and symptoms severity were individually recorded. Rats were weighted at the arrival, before, and after each 4 h exposure and before euthanasia.

BALF analysis

Rats ($n = 6$) were euthanized 24 h after the last exposure end and bronchoalveolar lavages were performed with PBS. A first bronchoalveolar lavage was performed using 5 mL of PBS. Two other lavages were then performed with 10 mL of PBS to collect more cells. Collected BALF were centrifuged at 350 g (4 °C) for 10 min.

[1]LLOQ: lower limit of quantification.

Cell pellets of the three lavages were suspended in Hank's Balanced Salt Solution (HBSS) and immune cells were counted with Cellometer auto2000 (Ozyme, Saint-Cyr-l'École, France) using propidium iodide and orange acridine. BALF cytospins were prepared by methanol fixation and May-Grünwald Giemsa staining (MGG) to allow immune cells differential count (macrophages, lymphocytes, polymorphonuclear neutrophils (PMN), polymorphonuclear eosinophils (PME), and polymorphonuclear basophils (PMB)).

Supernatants recovered from the first lavage were aliquoted and stored at −80 °C until biochemical analysis. BALF lactate dehydrogenases (LDH) and total proteins contents were assessed using commercial kits (respectively, 74048 and 74230, Siemens Healthineers, Erlangen, Germany). Absorbances were measured at, respectively, 340/410 nm for LDH and 596/694 nm for total proteins on ADVIA 1800 clinical chemistry automaton (Siemens Healthineers). BALF pro-inflammatory cytokines were quantified by ELISA assay. IL-1β, TNF-α, and IL-6 concentrations (respective LLOQ= 6 pg/mL, 16 pg/mL, and 13 pg/mL) were measured using Bio-Plex Pro™ Rat kit (64178837, Bio Rad, Hercules, CA, USA). GRO/KC, INF-γ, and MIP-2 concentrations (respective LLOQ = 19.7 pg/mL, 6.2 pg/mL, and 11.3 pg/mL) were measured using Milliplex MAP Rat kit (RECYTMAG-65K, Merck, Kenilworth, NJ, USA). Measurements were performed on Bio-Plex® MAGPIX™ System (Bio Rad). 8-Isoprostane (8-iso PGF2α) levels in BALF were quantified using ELISA assay (ADI-900-010, Enzo, LLOQ= 6.1 pg/mL). Measurements were performed on Multiskan Go plate reader (Thermo Scientific, Waltham, MA, USA) at 405 nm.

Lungs histopathology

After euthanasia, rats ($n = 3$) were perfused with PBS then with 4% formalin. Injections of 4% formalin were also performed directly inside the lungs to inflate them. After 48 h incubation in 4% formalin, lungs were transferred to PBS and included in paraffin. Five micro-meter slices were cut from paraffin blocks with Autocut 2045 (Leica, Norcross, GA, USA) and stained with hematoxylin, phloxine, and saffron (HPS staining). Lungs histopathology study was carried out on cranial lobes of right lungs to insure reproducibility. Samples were observed under DMI6000B light microscope (Leica) with a DFC 450 C color camera (Leica).

After staining, microscopy slides were sent to Novotec R&D (Bron, France) who performed anatomo-histopathological reading and lesions scoring. Localization (alveolar, vascular or bronchial) and severity of pulmonary lesions resulting from exposures were assessed (Table 1) and lesion scores were calculated individually. Lesion scores means for each experimental group are presented in arbitrary units (A.U.).

Table 1. Novotec scoring and corresponding pulmonary lesions.

Lesion score	Observed lesions
0	No lesion or physiological lesions
1	Vascular lesions
2	Limited to moderate vascular and alveolar lesions, with or without bronchial lesion
3	Significant vascular and alveolar lesions, with or without bronchial lesion

8-OHDG immunofluorescence labeling in situ on rat lung

To perform lungs immunofluorescence labeling, 5 µm lungs slices were cut from paraffin blocks with Autocut 2045 (Leica). After toluene dewaxing, citrate buffer (pH 6; 10 mM; C9999, Sigma-Aldrich, St. Louis, MO, USA) incubation enable antigen unmasking. To reduce lung tissue autofluorescence (Davis et al. 2014), samples were stained with Sudan black (0.3%; 30 min; 199664, Sigma-Aldrich). Cells were then permeabilized with Triton X100 (0.025%; 10 min; X100, Sigma-Aldrich) and aspecific sites saturation was performed using bovine serum albumin (BSA; 6%; 1 h; A2153, Sigma-Aldrich). Lung slices were then incubated with primary antibody overnight at 4 °C (anti-8-OHdG antibody, Abcam ab48508; dilution 1/400), before shorter incubation (2 h) with secondary antibody (goat anti-mouse IgG secondary antibody, Life Technologies A11029; dilution 1/500). Finally, slides were mounted using Vectashield© Hardset containing Di Aminido Phenyl lndol (DAPI; H-1500,Vector). Lung sections without primary antibody incubation were used as negative controls to ensure specificity of observed labeling.

Statistical analysis

Results are presented as means ± standard deviations (SD) for each experimental group. Statistical analysis was performed using GraphPad Prism 7 software (GraphPad Software, La Jolla, CA). Within the same exposure scenario, comparison with the control group (air) or other experimental groups means was performed using one-way ANOVA variance tests and Tukey's post-tests. To compare exposure scenarios for the same aerosol two-way ANOVA variance tests and Sidak's post-tests were implemented. Two-way ANOVA variance tests and Dunnett's post-tests were used to compare weights losses of rats to the control ones. Statistical analysis was performed using an α-risk of 0.05 and the p-value was used to assess differences significance. p-values were represented on figures using stars or circles (* or ° p-value < 0.05, **or °° p-value < 0.01, ***or °°° p-value < 0.001, ****or °°°° p-value < 0.0001).

Results

Aerosols physico-chemical characterization

Transmission electron microscopy (TEM) observations showed micronic spherical agglomerates of Al_2O_3NPs from bulk powder (Figure 2(A)). To characterize alumina crystalline structure, XRD experiments were performed on bulk powder. Results confirmed majority of γ and δ polymorphs as indicated by the supplier (Figure 2(B)).

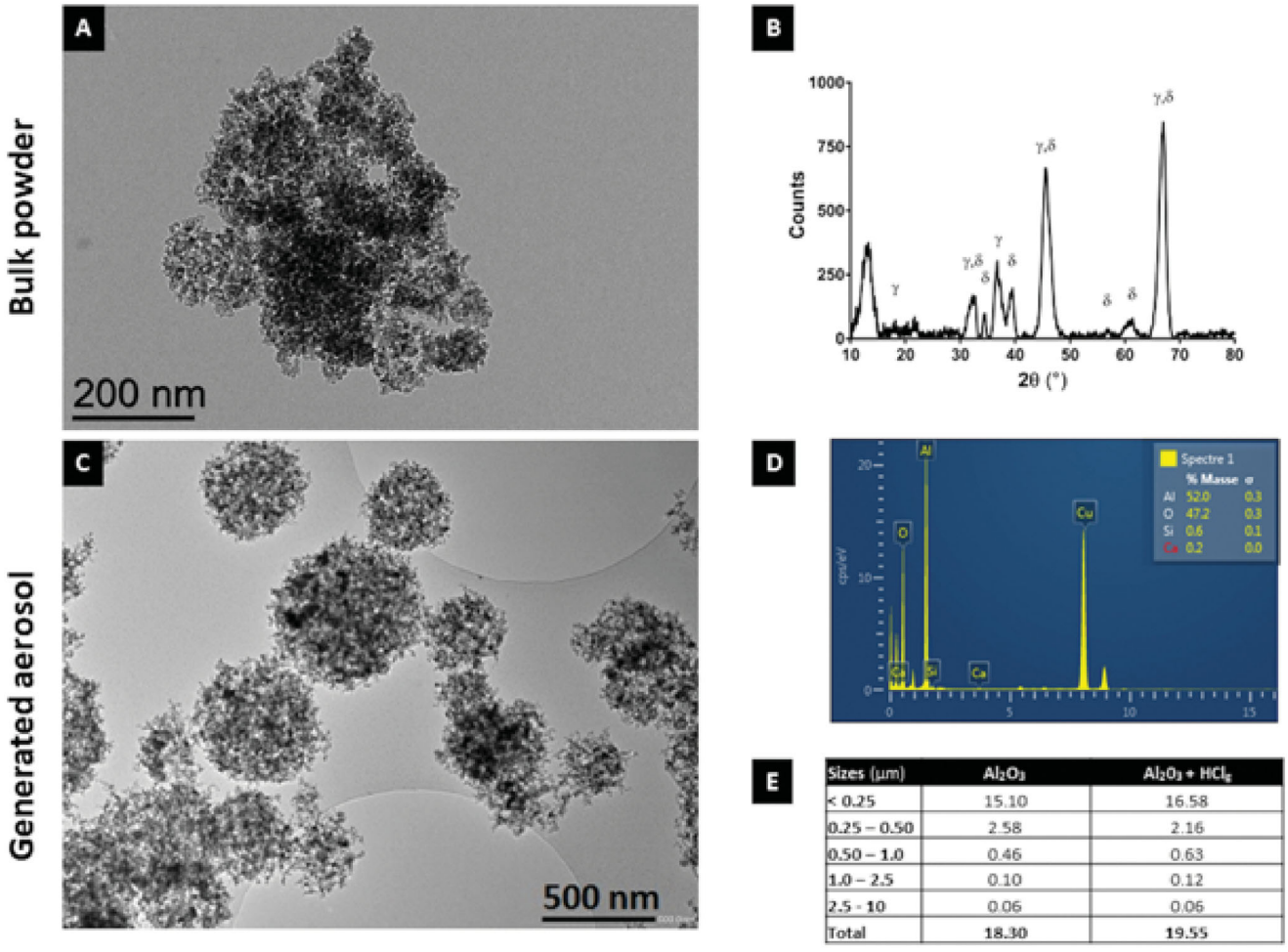

Sizes (µm)	Al_2O_3	$Al_2O_3 + HCl_g$
< 0.25	15.10	16.58
0.25 – 0.50	2.58	2.16
0.50 – 1.0	0.46	0.63
1.0 – 2.5	0.10	0.12
2.5 - 10	0.06	0.06
Total	18.30	19.55

Figure 2. Bulk powder and aerosols alumina nanoparticles physico-chemical characterization. Transmission electron microscopy (TEM) images of Al_2O_3 NPs in bulk powder (A) and generated aerosol (C) (respective scale bars = 200 nm and 500 nm). Crystalline phases (γ and δ) identification using X-ray diffraction (XRD) on bulk Al_2O_3 NPs (B). NPs elementary chemical composition (in %) using energy-dispersive X-ray (EDX) spectroscopy on Al_2O_3 NPs aggregates retrieved in the generated aerosol (D). Table E summarizes Al_2O_3 NPs representative particles size distribution in the generated aerosols measuring using Sioutas cascade impactor (mg/m^3 for each size class in µm).

Once nebulized, Al_2O_3 NPs formed spherical agglomerates (Figure 2(C)). The presence of HCl_g did not modify the shape of agglomerates in aerosols (data not shown). Energy dispersive X-ray (EDX) analysis confirmed aluminum and oxygen atoms presence without chemical impurities. The copper spike on EDX spectra corresponds to TEM grids used for aerosol sampling (Figure 2(D)). Results obtained with Sioutas (SKC Inc., Seoul, South Korea) cascade impactor revealed that a majority of particles in the agglomerates in generated aerosols had a size below 250 nm (Figure 2(E)). Mean aerodynamic diameters of 383.07 nm and 343.59 nm were, respectively, calculated for Al_2O_3 NPs aerosol and for the mixture aerosol. Based on these data, the presence of HCl_g did not seem to modify particles' concentrations and size distribution over 250 nm (Figure 2(E)).

To deepen and complete these analytical data, the content of aerosol particles was assessed using Al quantification (ICP-OES) after filter samplings. Mean Al_2O_3 concentrations of 22.1 ± 4.5 mg/m^3 and 20.0 ± 2.9 mg/m^3 were, respectively, measured for aerosols containing Al_2O_3 NPs and Al_2O_3 NPs associated with HCl_g (Table 2A). Therefore, we confirmed that the addition of HCl_g to aerosol did not significantly modify NPs concentrations. HCl_g concentrations in generated aerosols were estimated through the measurements of chlorine (Cl^-) levels carried out on filters (particulate fraction) and bubbler (free fraction) samples. Results showed 10 times smaller Cl^- levels than target concentrations (5 ppm = 7.4 mg/m^3). The addition of Al_2O_3 NPs to the HCl_g aerosol did not seemed to modify significantly Cl^- levels but this statement should be taken cautiously due to the variability in the chloride measurements. However, it has to be noted that in the presence of Al_2O_3 NPs, Cl^- in the aerosols was exclusively found in particulate fraction whereas it was exclusively in free fraction when alone (Table 2B). Moreover, variations in Cl^- concentrations were noted when HCl_g was alone, with concentrations ranging from 0 to 2145 µg/m^3 (Table 2B). These variations were not observed in presence of Al_2O_3 NPs.

Lungs aluminum content increasing after repeated exposures

Pulmonary aluminum load was measured by ICP-OES after aerosols inhalation. Following single exposures (SE) to Al_2O_3 NPs alone or associated with HCl_g, concentrations around 100 µg of aluminum per g of lung were measured (Figure 3).

Table 2. Generated aerosols alumina and HCl_g contents.

A

Aerosol	Al (µg/filter)[a]	Al concentration (mg/m^3)[b]	Al_2O_3 concentration (mg/m^3)[c]	Al_2O_3 concentration mean ± SD (mg/m^3)
Al_2O_3	137	9.1	17.3	22.1 ± 4.5
	183	12.2	23.0	
	207	13.8	26.1	
Al_2O_3 + HCl_g	185	12.3	23.3	20.0 ± 2.9
	147	9.8	18.5	
	144	9.6	18.1	

B

	Particulate fraction (filters)		Free fraction (bubblers)			
Aerosol	Cl^- (µg/filter)	Cl^- (µg/m^3)[A]	Cl^- (µg/bubbler)	Cl^- (µg/m^3)[A]	Cl^- total concentrations (µg/m^3)[B]	Cl^- total concentrations mean ± SD (µg/m^3)
HCl_g	–	–	32.2	**2145**	**2145**	**791 ± 1178**
	–	–	3.4	**228**	**228**	
	–	–	0	**0**	**0**	
Al_2O_3 + HCl_g	8.9	**596**	0	**0**	**596**	**617 ± 32**
	9.0	**601**	0	**0**	**601**	
	9.8	**653**	0	**0**	**653**	

[a]After white deduction.
[b]Sampling at 1 Lpm for 15 min (/0.015).
[c]× 1.889.
Table A shows alumina (Al_2O_3) mean mass concentrations in the generated aerosols. Aluminum mass was measured on three different filters (µg/filter). Based on these results, aluminum and alumina concentrations in aerosols (mg/m^3) were calculated and alumina mean mass concentrations (mg/m^3) were determined for each experimental aerosol. Table B shows chlorine mean concentrations in the generated aerosols. Chlorine particulate and free fractions were, respectively, measured on three filters and bubbler samples (µg/filter or µg/bubbler). Corresponding chlorine mass concentrations were calculated (µg/m^3) and were added to determine total chlorine levels (µg/m^3). Total chlorine mean mass concentrations (µg/m^3) were calculated for each experimental aerosol. Bold values refer to chlorine mass concentrations in µg/m^3.
[A]Sampling at 1 Lpm for 15 min (/0.015).
[B]Particulate fraction + free fraction.

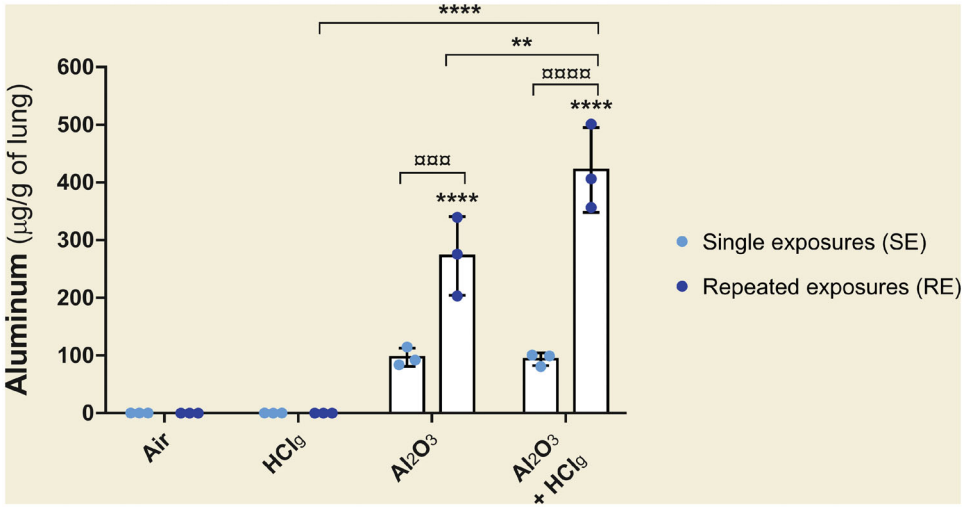

Figure 3. Pulmonary aluminum deposition after nose-only exposures. Rats were exposed to air, HCl_g, Al_2O_3 or to the mixture Al_2O_3 + HCl_g. Clear blue points symbolize single exposures (SE) and dark blue points symbolize repeated exposures (RE) to each aerosol. Mean aluminum quantities (µg/g of lung) ± SD were measured in lungs 24 h after the last exposure using inductively coupled plasma optical emission spectrometry (ICP-OES). One-way ANOVA and Tukey's post-test ($n = 3$, ** p-value < 0.01, **** p-value < 0.0001, α risk = 0.05) were performed to compare each experimental condition to the control within the same exposure scenario and Two-way ANOVA and Sidak's post-test ($n = 3$, ¤¤¤p-value < 0.001, ¤¤¤¤ p-value < 0.0001, α risk = 0.05) were performed to compare the two exposure scenarios for the same aerosol.

However, these mean quantities were not significantly different from air exposed animals. Repeated exposures (RE) to Al_2O_3 NPs alone or in association with HCl_g-induced significant aluminum quantities increases in lungs compared to air exposed rats or to those exposed to the same conditions in SE (Figure 3). RE to Al_2O_3 NPs with HCl_g significantly increased pulmonary aluminum load compared to repeated exposures to each component alone (Figure 3).

Table 3. Rats body weight changes during the experimental period.

A			4 h (AE)	28 h (BS)
Single exposure (SE)	Air	Mean (g) ± SD	−16.1 ± 4.6	−1.2 ± 5.7
		SA		
	HCl_g	Mean (g) ± SD	−16.5 ± 4.8	−3.4 ± 3.7
		SA	ns	Ns
	Al_2O_3	Mean (g) ± SD	−13.1 ± 3.8	−4.5 ± 4.1
		SA	ns	*
	$Al_2O_3 + HCl_g$	Mean (g) ± SD	−15.2 ± 2.8	−3.9 ± 2.7
		SA	ns	Ns

B			4 h (AE)	24 h (BE)	28 h (AE)	48 h (BE)	52 h (AE)	72 h (BE)	76 h (AE)	100 h (BS)
Repeated exposure (RE)	Air	Mean (g) ± SD	−15.7 ± 2.9	−5.0 ± 4.0	−21.2 ± 3.0	−9.0 ± 4.0	−23.6 ± 3.9	−9.9 ± 5.2	−21.1 ± 4.1	−10.0 ± 5.2
		SA								
	HCl_g	Mean (g) ± SD	−18.6 ± 3.5	−1.5 ± 2.1	−20.9 ± 3.1	−3.5 ± 2.6	−22.5 ± 4.2	−4.4 ± 3.5	−22.5 ± 4.4	−2.8 ± 4.5
		SA	ns	ns	ns	**	Ns	**	ns	****
	Al_2O_3	Mean (g) ± SD	−12.8 ± 2.1	−4.5 ± 3.4	−15.3 ± 4.6	−7.5 ± 6.0	−18.6 ± 6.0	−9.6 ± 6.8	−21.8 ± 5.1	−8.7 ± 8.3
		SA	ns	ns	**	Ns	**	Ns	ns	ns
	$Al_2O_3 + HCl_g$	Mean (g) ± SD	−15.3 ± 3.3	−2.6 ± 2.1	−15.3 ± 2.6	−2.4 ± 2.7	−15.2 ± 3.7	−2.9 ± 3.3	−13.9 ± 5.0	−3.2 ± 4.3
		SA	ns	ns	**	***	****	****	****	***

Rats were exposed once or repeatedly to air, HCl_g, Al_2O_3 or to the mixture $Al_2O_3 + HCl_g$. Rats body weight change (in gram, mean ± SD) was measured before and after each aerosol exposure. Obtained results during single exposures (SE) and during repeated exposures (RE) are, respectively, presented in Tables A and B. Tables show variations from initial body weight (t_0, before the first exposure) before each exposure (BE, 24 h (B), 48 h (B), 72 h (B)), after each exposure (AE, 4 h, 28 h (B), 52 h (B), 76 h (B)) and before sacrifice (BS, 28 h (A) and 100 h (B)). Two-way ANOVA and Dunnett's post-test ($n = 12$, *p-value < 0.05, **p-value < 0.01, ***p-value < 0.001, ****p-value < 0.0001, α risk $= 0.05$) were performed as statistical analysis (SA) to compare body weights variation compared with initial body weights (t0) in each experimental condition with the control group (air). AE: after exposure; BE: before exposure; BS: before sacrifice; SA: statistical analysis; ns: not significant.

Clinical symptoms and body weight

Animal clinical follow-up did not highlight any treatment-related clinical symptom following exposures. Moreover, even if exposures (including air) induced significant animals weight losses, no biologically relevant change in body weight were observed after SE (Table 3A) and RE (Table 3B). Indeed, these weight decreases were always less than 10% of rats' initial weight (data not shown) and no particular trend was noted for the different experimental groups (Table 3).

Alveolar–capillary barrier and pulmonary inflammation

No change in total proteins or lactate dehydrogenases (LDH) concentrations was observed following SE compared to air exposed rats (Figure 4(A,B)). Only RE to Al_2O_3 NPs alone or associated to HCl_g induced significant concentrations increases of total proteins and LDH in rats BALF compared to air exposed control animals (Figure 4(A,B)). Total protein concentrations of 0.18 ± 0.03 g/L and 0.22 ± 0.04 g/L and LDH concentrations of 99 ± 43 U/L and 112 ± 42 U/L were measured in rats BALF following, respectively, RE to Al_2O_3 NPs and toAl_2O_3 NPs + HCl_g.

The number of total cells was increased in rats BALF after RE to Al_2O_3 NPs. Moreover, significantly higher total cell numbers were counted following RE than SE to Al_2O_3 NPs and to Al_2O_3 NPs + HCl_g aerosols (Figure 4(C)). RE to the same aerosols also induced significant polymorphonuclear neutrophils (PMN) number increases in BALF compared to air exposed control animals (Figure 4(D)). In contrast, no significant change in macrophages and lymphocytes numbers was highlighted by the carried out counts (Figure 4(E,F)).

RE to Al_2O_3 NPs or Al_2O_3 NPs + HCl_g aerosols led to significant TNF-α and IL-1β concentration increases in rats BALF (Figure 5(A,B)). TNF-α concentrations of 42.86 ± 13.07 pg/mL and 45.73 ± 11.77 pg/mL, and IL-1β concentrations of 456.2 ± 163.2 pg/mL and 341.6 ± 58.11 pg/mL were, respectively, measured. Significant increased concentrations of GRO/KC and MIP-2 were also measured in rats BALF after, respectively, RE to Al_2O_3 NPs (Figure 5(C)) and SE to Al_2O_3 NPs (Figure 5(D)) compared to air exposed control rats.

Histopathology observations

Lung parenchyma observations revealed the presence of pathological lesions following experimental aerosols inhalation (Figure 6). However, no peribronchial or perivascular fibrosis, resorption hyperplasia (phagocytosis phenomena), or pleura inflammation was reported in this study. Lesions scoring (Novotec R&D, Cincinnati, OH, USA) was performed in order to compare the different experimental aerosols and exposure scenarios' effects (Figure 7). No statistical analysis was performed on these data as groups were composed of only three animals and scores are not a measured biological data (values estimated from observations and without unit). A table with scoring details including lesions localizations is provided as Supplementary data.

In the lungs of control rats, vascular congestions were occasionally found and considered as physiological lesions (histological alteration which would have no functional consequence and which can be observed in normal tissue, Figure 6(A,B)). HCl_g exposures mainly induced vascular lesions. SE increased vascular congestions (Figure 6(C)), while RE induced vascular edema and, in some cases, velamentous epithelium, pneumocytes edema, and moderate walls thickening were observed in the alveolar regions (Figure 6(D)). Al_2O_3NPs inhalation mainly induced alveolar interstitial and inflammatory lesions (Figure 6(E,F)). Indeed, marked interalveolar septum edemas were found within rats pulmonary epithelium after SE and RE. Slight bronchial

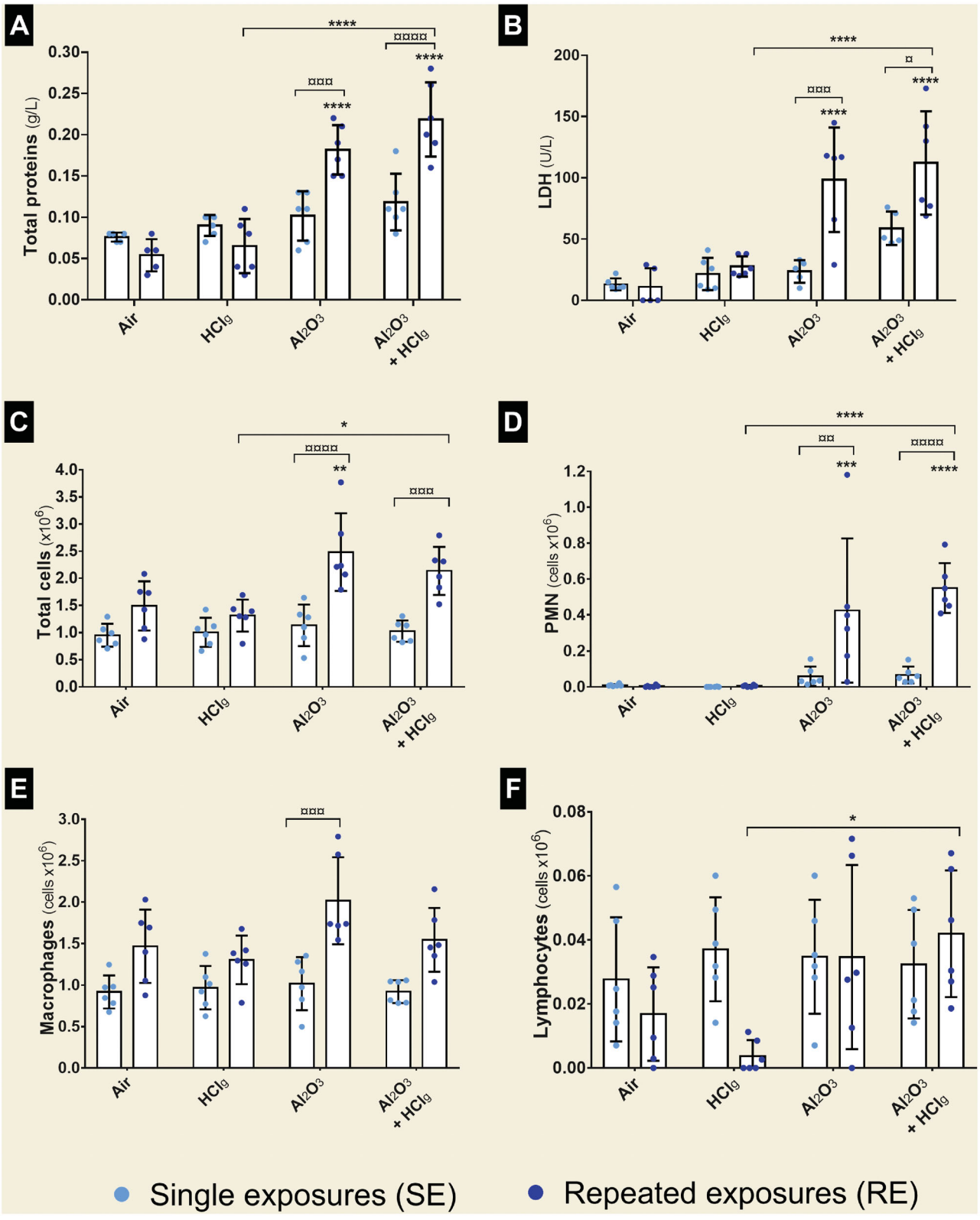

Figure 4. Total proteins, LDH and immune cells populations in bronchoalveolar lavage fluids (BALF). Rats were exposed to air, HCl_g, Al_2O_3 or to the mixture Al_2O_3 + HCl_g. Clear blue points symbolize single exposures (SE) and dark blue points symbolize repeated exposures (RE) to each aerosol. Total proteins (g/L) (A) and lactate dehydrogenases (LDH, U/L) (B) concentrations were measured in rats BALF 24 h after the last exposure. Total cells, polymorphonuclear neutrophils (PMN), macrophages and lymphocytes (cells $\times 10^6$) were counted on BALF cytospins (respectively C, D, E, and F). Results are expressed as mean values ± SD. One-way ANOVA and Tukey's post-test ($n = 6$, * p-value < 0.05, ** p-value < 0.01, *** p-value < 0.001, **** p-value < 0.0001, α risk $= 0.05$) were performed to compare each experimental condition to the control within the same exposure scenario and two-way ANOVA and Sidak's post-test ($n = 6$, ° p-value < 0.05, °° p-value < 0.01, °°° p-value < 0.001, °°°° p-value < 0.0001, α risk $= 0.05$) were performed to compare the two exposure scenarios for the same aerosol.

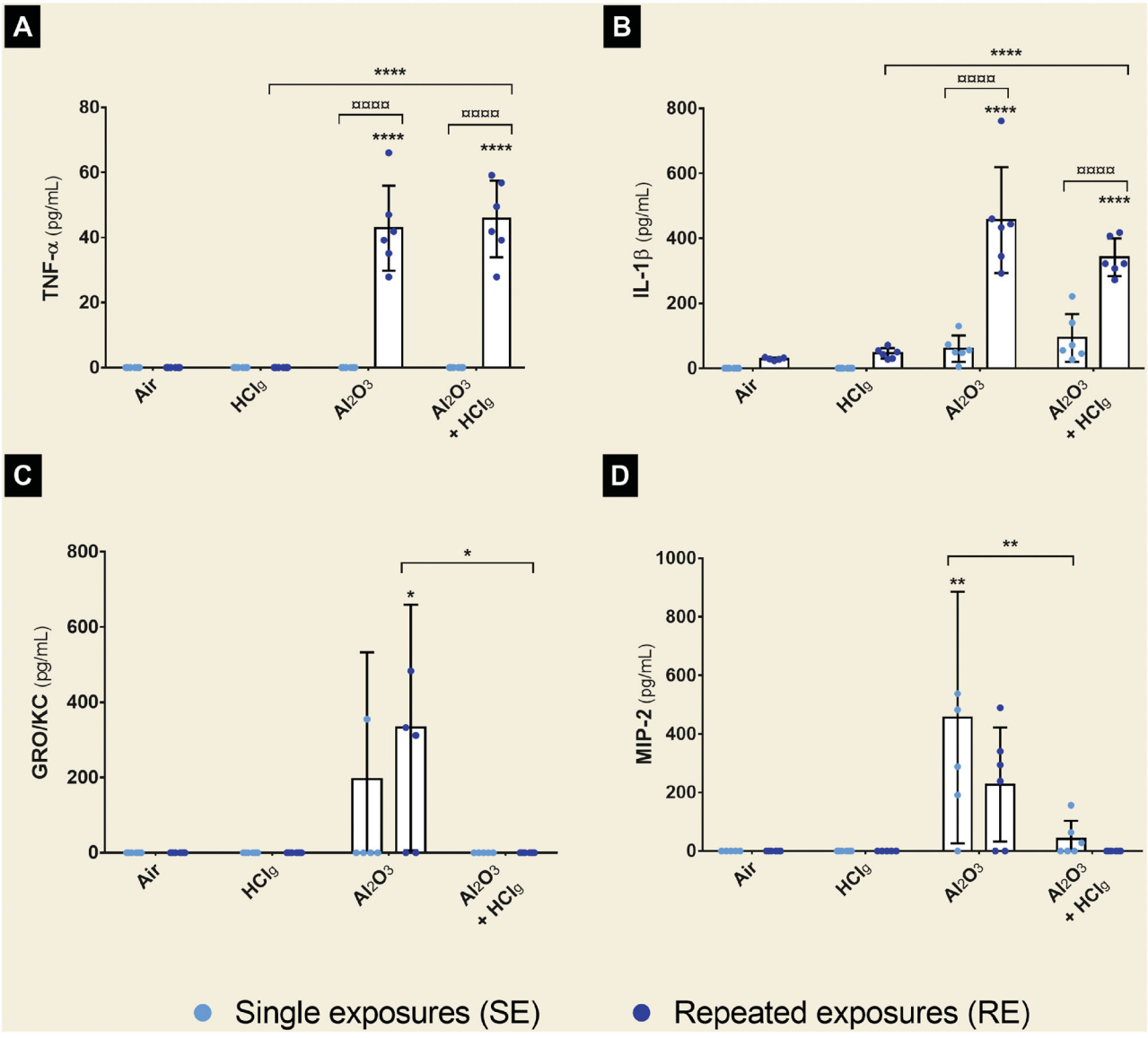

Figure 5. Aerosols pro-inflammatory potential on rat lungs after nose-only inhalations. Rats were exposed to air, HCl_g, Al_2O_3 or to the mixture $Al_2O_3 + HCl_g$. Clear blue points symbolize single exposures (SE) and dark blue points symbolize repeated exposures (RE) to each aerosol. Pro-inflammatory cytokines concentrations (pg/mL) of TNF-α (A), IL-1β (B), GRO/KC (C) and MIP-2 (D) were measured in rats BALF 24 h after the last exposure by ELISA multiplex. Results are expressed as mean values ± SD. One-way ANOVA and Tukey's post-test ($n = 6$, * p-value < 0.05, ** p-value < 0.01, **** p-value < 0.0001, α risk $= 0.05$) were performed to compare each experimental condition to the control within the same exposure scenario and two-way ANOVA and Sidak's post-test ($n = 6$, ¤¤¤¤ p-value < 0.0001, α risk $= 0.05$) were performed to compare the two exposure scenarios for the same aerosol.

pre-exfoliation phenomena (Figure 6(E)) and vascular edemas (Figure 6(F)) were also observed. In some cases, localized inflammatory areas, composed of polymorphonuclear cells and lymphocytes, were also found in rats' lungs (Figure 6(F)). Co-exposures to Al_2O_3 NPs and HCl_g induced vascular and bronchial interstitial lesions at a time (Figure 6(G,H)). Marked bronchial pre-exfoliation phenomena (Figure 6(G)), vascular, and interalveolar septum edemas (Figure 6(G)) were found in rats' lungs after SE. RE to the same aerosol mainly induce vascular edemas and interalveolar septum edemas were observed in some animals but no bronchial lesions was reported (Figure 6(H)). Moreover, in one animal, repeatedly exposed to mixture pre-pulmonary edema stage was observed (significant vascular edema, dilated capillaries, and incipient alveolar septa rupture). Therefore, higher mean lesion scores were calculated in animals exposed to aerosols containing Al_2O_3 NPs alone or associated with HCl_g (Figure 7).

In conclusion, results did not suggest major influence of exposure scenario toward histopathological lesions induction as close scores were calculated for SE and RE to the same aerosol. The presence of Al_2O_3 NPs in the aerosol induced lung irritation increasing lesion score, but adding HCl_g to Al_2O_3 NPs aerosol did not seem to worsen lesions comparing to those resulting from Al_2O_3 NPs inhalation alone. An exception was noted for SE as the addition of HCl_g to Al_2O_3 NPs aerosol lead to bronchial lesion worsening.

Oxidative stress analysis

To assess oxidative stress induction following experimental aerosols exposures, 8-OHdG (8-hydroxy-2′-deoxyguanosine,

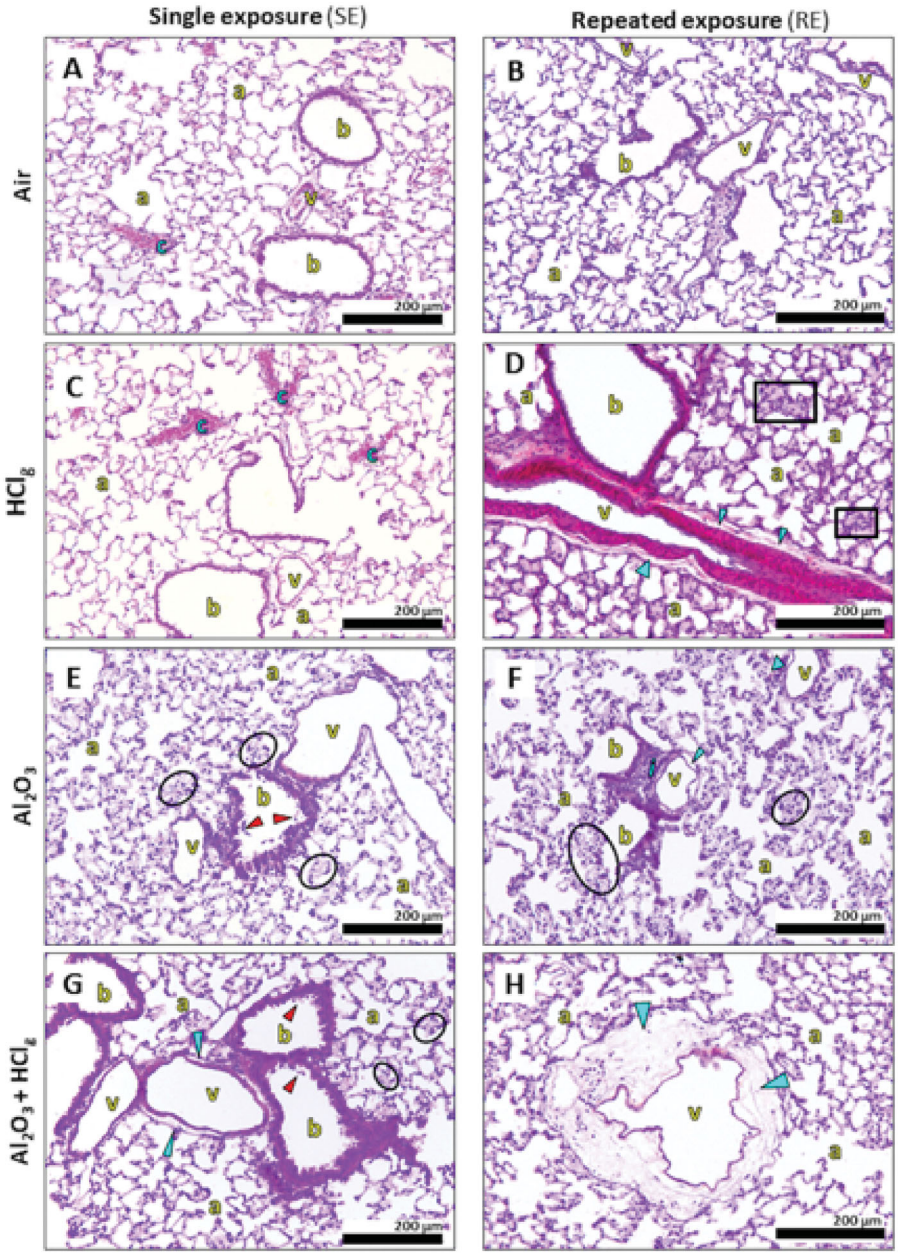

Figure 6. Pulmonary histopathological lesions observations following inhalation exposures. Rats lung parenchyma stained in HPS were observed in optical microscopy for histopathological analysis. Images show, respectively, lung parenchyma 24 h after single exposure (SE) to air (A), HCl_g (C), Al_2O_3 (E) and Al_2O_3 + HCl_g (G) and 24 h after repeated exposures (RE) to air (B), HCl_g (D), Al_2O_3 (F) and Al_2O_3 + HCl_g (H). Scale bar = 200 µm. Pictures legends: a = alveoli; b = bronchioles or bronchi; v = blood vessel; c = vascular congestion; blue arrows = vascular edema; red arrows = bronchial (pre)-exfoliation; *i* = inflammatory area; black squares = velamentous epithelium and black circles = interalveolar septum edema.

oxidative nucleic acids' damages marker) was labeled *in situ* in the lung tissue of the rats using immunofluorescence. Microscopic observations revealed 8-OHdG fluorescent signal after SE (Figure 8(A–D)), whereas no specific signal was observed after RE to the different aerosols. After SE to the experimental aerosols, cytoplasmic and nuclear labeling were found both in alveolar (Figure 8(B,D)) and bronchial epithelia (Figure 8(C)). Aerosols containing Al_2O_3 NPs ± HCl_g seemed to induce more labeling on bronchial regions than on alveolar regions whereas HCl_g alone lead to both bronchial and alveolar labeling. However, no quantitative analysis was performed to compare labeling in the two regions. These labeling localizations referred to RNA (cytoplasmic) and DNA (nuclear) oxidations.

To complete our investigations on oxidative stress induced by inhalations, 8-isoprostane (lipid peroxidation marker) concentrations were measured in rats BALF 24 h after the last exposure end. Results did not reveal any significant increase in 8-isoprostane concentrations following inhalations (Figure 8(E)). Significant 8-isoprostane concentration decreases were measured after RE to Al_2O_3 NPs and to Al_2O_3 NPs + HCl_g compared to control, with respective mean values of 26.6 ± 1.5 pg/mL and 24.4 ± 1.7 pg/mL versus 34.9 ± 4.7 pg/mL for the control group (Figure 8(E)).

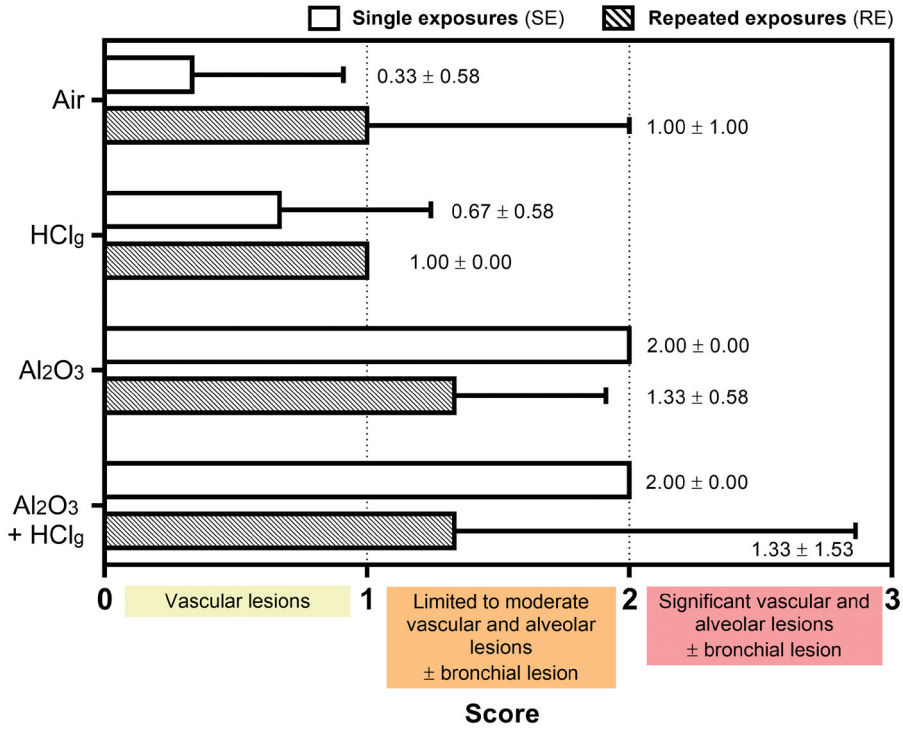

Figure 7. Pulmonary histopathological lesions scoring. Rats were exposed to air, HCl_g, Al_2O_3 or to the mixture $Al_2O_3 + HCl_g$. Scoring was performed on HPS stained lungs slices of three rats of each group. Lesion scores (mean ± SD, $n = 3$) were estimated for each experimental aerosol and exposure scenario based on the presence and the gravity of vascular, alveolar and bronchial lesions observed in rats lungs 24 h after the last exposure. Empty and striped bars represent, respectively, single exposures (SE) and repeated exposures (RE) results.

Discussion

A combined study of gas and particles toxicity is an innovative concept. In this pilot study, nose-only inhalation system was selected to ensure better control of the inhaled dose. Only one dose of HCl_g and Al_2O_3 NPs could be assessed. In the case of Al_2O_3 NPs, a high dose was used (10 g/L suspension leading to 20.0–22.1 mg/m^3 aerosol) to ensure biological response following inhalation in order to identify toxic effects.

However, this choice could have masked subtle HCl_g effects on Al_2O_3 NPs when mixed together. Indeed, observed effect in this study could mainly be due to the delivered Al_2O_3 NPs load to the lungs, especially since HCl_g measured concentrations in the experimental aerosols were lower than expected (617–791 µg/m^3 versus 5 ppm = 7.4 mg/m^3). This difference and the experimental variability in chlorides dosing repetitions could be explained by both HCl_g high reactivity with water, leading to HCl_g dissolution in water drops on the exposure system walls, and bubblers saturation by other compounds, sometimes causing a non-optimal chlorides trapping. Moreover, in our study, Al_2O_3 NPs were nebulized from a NPs suspension in water. This method is different from combustion process in a solid composite propellant and could promote aggregates formation. We can, therefore, assume that animals were exposed to particles aggregates with different size distributions than those which could be found on the field.

Specific physico-chemical characterization is a mandatory step to better understand the biological effects of mixture aerosols. Their characterization revealed the presence of spherical Al_2O_3 NPs agglomerates with respective mean aerodynamic diameters of 383 nm for Al_2O_3 NPs alone and of 344 nm for mixtures. Al_2O_3 NPs concentrations in aerosols were high and comprised between 20.0 mg/m^3 and 22.1 mg/m^3. Indeed, Paur and colleagues reported in their literature review that 5 mg/m^3 could be considered as an upper limit for workplace NPs mass concentration, according to Occupational Safety and Health Administration (OSHA) standard for respirable nuisance dust (Paur et al. 2011). Based on this value, they estimated a mass of NPs per surface area deposition in human lungs of 5×10^{-3} µg/cm^2/h, which would correspond in our exposure scenarios to theoretical particles deposition in human lungs of 0.02 µg/cm^2 ($5 \times 10^{-3} \times 4$) after SE and of 0.08 µg/cm^2 ($5 \times 10^{-3} \times 16$) after RE. Considering alveolar surface of 4000 cm^2 in rats, exposures to NPs aerosols led to higher measured pulmonary depositions. Indeed, for Al_2O_3 NPs exposures, values of 0.04 µg/cm^2 and 0.13 µg/cm^2 were, respectively, obtained for SE and RE, while concentrations for co-exposures with HCl_g were, respectively, 0.03 µg/cm^2 and 0.18 µg/cm^2. Therefore, these experimental values are higher than theoretical values but consistent with aerosols high NPs concentrations. Even if we observed high NPs pulmonary depositions, these scenarios are relevant in a context of accidental exposures where specific workers (e.g. military or aerospace industry personnels) could be exposed to combustion aerosols.

To quantify Al_2O_3 NPs biodistribution in lungs after exposures, aluminum concentrations were measured using ICP-OES. Obtained values were approximately four times higher in lungs after RE compared to SE. These results are

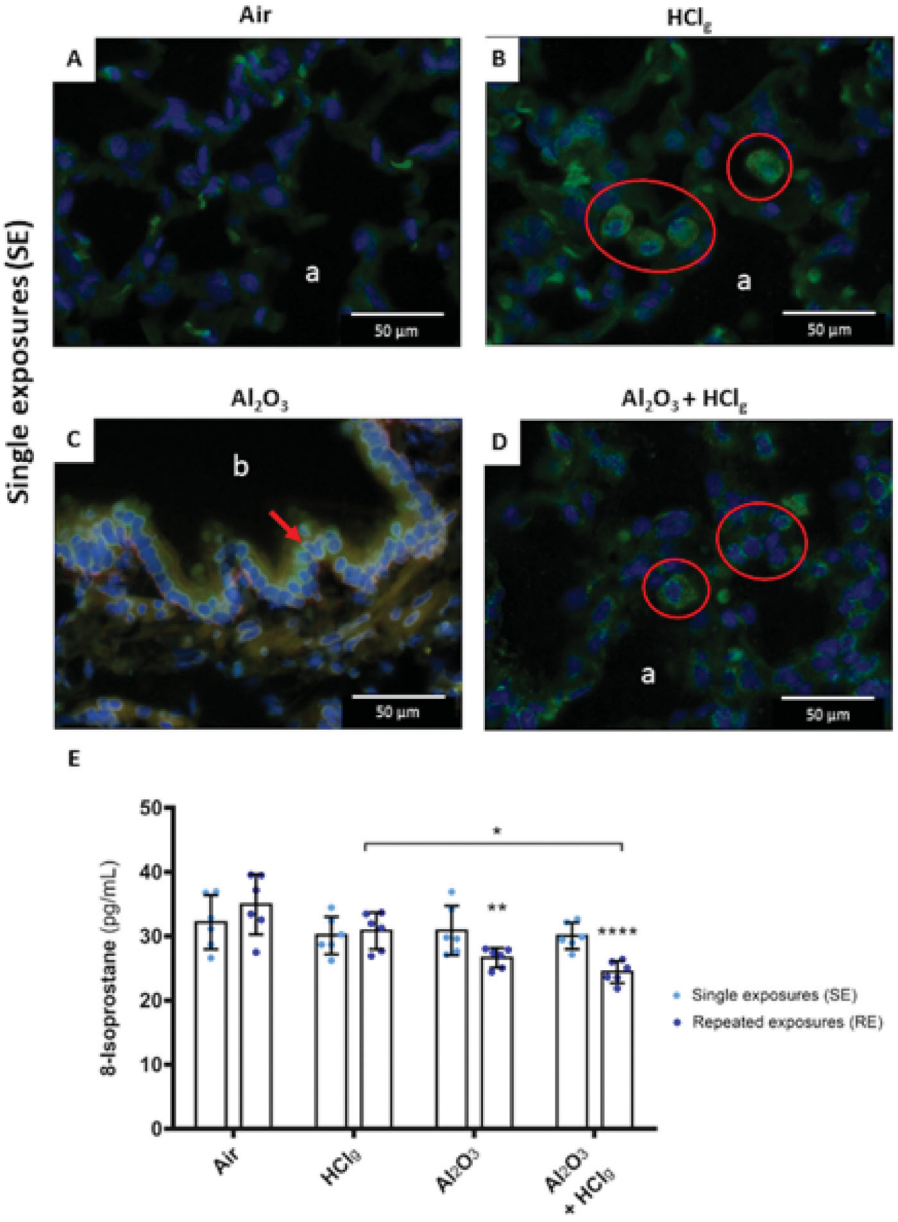

Figure 8. Oxidative stress induction by experimental aerosols inhalation exposures. Immunofluorescence was performed to detect 8-OHdG (8-hydroxy-2′-deoxyguanosine, green fluorescence) on rat lungs slices 24 h after the last exposure. DNA was stained by DAPI, which emits in blue fluorescence. Pictures represent obtained results following single exposures (SE) to air (A), HCl_g (B), Al_2O_3 (C) and $Al_2O_3 + HCl_g$ (D). Scale bars = 50 µm. Pictures legends: a = alveoli; b = bronchioles or bronchi. Red blood cells could also emit in green fluorescence, but red arrows and red circles point out specific 8-OHdG staining. 8-Isoprostane concentrations (pg/mL) were measured in rats BALF 24 h after the last exposure (E). Clear blue points symbolize single exposures (SE) and dark blue points symbolize repeated exposures (RE) to each aerosol. Results are expressed as mean values ± SD. One-way ANOVA and Tukey's post-test ($n = 3$, * p-value < 0.05, ** p-value < 0.01, **** p-value < 0.0001, α risk $= 0.05$) were performed to compare each experimental condition to the control within the same exposure scenario and two-way ANOVA and Sidak's post-test ($n = 3$, α risk $= 0.05$) were performed to compare the two exposure scenarios for the same aerosol.

consistent with exposure scenarios as RE correspond to four repetitions of SE. NPs accumulated in lungs after exposures and were still retained by lungs after 100 h in the case of RE, suggesting absence or slow clearance mechanisms early after Al_2O_3 NPs aerosols inhalation. However, in this study, rats were euthanized 24 h after the last exposure bringing no information about long-term Al_2O_3 NPs clearance. This result seems consistent with a study carried out on Sprague–Dawley rats by intratracheal instillations, which concluded to a very slow clearance, gradual accumulation, and pulmonary retention of alumina particles 19 weeks after repeated exposures (Schlesinger et al. 2000). Moreover, aluminum concentration was significantly increased in the case of co-exposure to Al_2O_3 NPs with HCl_g compared to Al_2O_3 NPs aerosols, while NPs concentration and size distribution were not modified. Therefore, we hypothesized that acidification of mixture aerosols may promote Al_2O_3 NPs dissolution (Franke et al. 1987), increasing aluminum pulmonary bioavailability. Indeed, in aqueous environment, Al_2O_3 NPs could hydrated and react with hydrogen ions to form water and aluminum ions as follow: $Al_2O_3 + 6\,H^+ \rightarrow 2\,Al^{3+} + 3\,H_2O$ (Diggle et al. 1970; Franke et al. 1987). Particles overload, especially after RE, and HCl_g local effect in lungs could also have both contribute to hinder particles

lungs clearance as previously shown in different studies (Lippmann et al. 1980; Pritchard 1989).

Pro-inflammatory properties of Al_2O_3 particles have already been reported in literature following inhalation (Sikkeland et al. 2016; Li et al. 2017; Kim et al. 2018). To date and to our knowledge, no literature data were found concerning the potential inflammatory response induced by HCl_g alone or Al_2O_3 NPs/HCl_g inhalation exposures. Therefore, we studied pro-inflammatory biomarkers following Al_2O_3 NPs, HCl_g or Al_2O_3 NPs/HCl_g mixtures nose-only exposures. Different secretion profiles were observed for each cytokine, depending on aerosol composition and exposure scenario. No increase of immune cells or cytokines concentrations was measured in animals BALF exposed to air or HCl_g. Our results showed early inflammation triggered by RE to aerosols containing Al_2O_3 NPs with or without HCl_g. Indeed, significant amount of alveolar macrophages and PMN were measured in BALF with increased secretion of IL-1β, TNF-α, and GRO/KC (except for Al_2O_3 NPs and HCl_g mixture). These results corroborate with histopathological observations with mainly interstitial and inflammatory lesions (localized areas composed of PMN and lymphocytes) in the case of Al_2O_3 NPs inhalation. Therefore, RE induced more potent pro-inflammatory response compared to SE. Increased cytokine concentrations observed in BALF also corroborate with PMN influx as they have chemoattractant properties (Huang et al. 1992; Toews 2001; Kim et al. 2018). IL-1β and TNF-α seem to orchestrate the pulmonary pro-inflammatory response. On the one hand, it has been described that Al_2O_3 NPs could stimulate the nuclear factor NFκB pathway (Simon-Vazquez et al. 2016). IL-1β concentration increases could thus be associated with this hypothesis, suggesting the inflammasome pathway involvement in the pulmonary pro-inflammatory response initiated by Al_2O_3 NPs. Indeed, the nuclear factor NFκB can contribute to the inflammasome regulation (Liu et al. 2017) which is involved in IL-1β synthesis (Lamkanfi and Dixit 2014). This conjecture is reinforced by the fact that this pathway is also known to be activated by pulmonary inflammation in patients with chronic obstructive pulmonary disease (Barnes 2016). On the other hand, Al_2O_3 NPs can also induce TNF-α release in BALF. This result corroborate with the study of Kim et al. which showed neutrophils, LDH, TNF-α, and IL-6 increased concentrations in BALF after Al_2O_3 NPs nose-only exposure of rats for 28 days (5 days/week) (Kim et al. 2018). TNF-α secretion after exposure to Al_2O_3 NPs may be linked to IL-1β release. Indeed, in a context of acute pulmonary inflammation, Saperstein and colleagues demonstrated that IL-1β contributes, in part, to TNF-α-mediated chemokine release, and neutrophil recruitment to the lung (Saperstein et al. 2009). Besides, in our study, GRO/KC and MIP-2 secretion in BALF were only measured after Al_2O_3 NPs exposure. These two cytokines possess neutrophils chemoattractant properties (Tanino et al. 2010). We hypothesized that co-exposure to Al_2O_3 NPs/HCl_g mixtures could modify their kinetic of secretions in BALF. A significant increase of MIP-2 concentrations was found in BALF only after SE to Al_2O_3 NPs. As a consequence, MIP-2 may act as an early step contributing to PMN recruitment. Furthermore, Pirela and colleagues also demonstrated down-regulation of GRO/KC and MIP-2 in the nasal lavage fluid after repeated whole-body inhalation exposure to printer-emitted engineered NPs in rats (containing aluminum oxide) (Pirela et al. 2019). Otherwise, IL-6 and INF-γ were not detected in BALF after SE and RE to the different aerosols of the study (respective detection limits: 13 pg/mL and 6.2 pg/mL). INF-γ promotes pulmonary inflammation through oxidative stress induction (Yin et al. 1999) and could have been secreted earlier than 24 h post-exposure to the aerosols, inducing nucleic acids oxidative damages (8-OHdG), which were still detected at that time. Therefore, we hypothesized that aluminum oxide-based nano-objects are notably able to induce secretion of different cytokine secretion profiles in BALF depending on their shape, time of exposure, and used inhalation system. Given the sensitizing properties of aluminum and HCl_g (Darmer et al. 1974; Cohen 2004; Zhu et al. 2013; Kongerud and Soyseth 2014), studies on immune effects could also be considered later (allergic response and other immune-related cytokines).

As oxidative stress is a physiological mechanism closely linked to pulmonary inflammation induced by NPs exposure, and indirectly to the increase of PMN number potentially releasing free radicals in the alveoli, this endpoint was investigated (Lugrin et al. 2014; Salzano et al. 2014; Khanna et al. 2015; Biswas 2016). Nucleic acids oxidation (8-OHdG) were only detected *in situ* following SE to HCl_g, Al_2O_3 NPs or mixture exposures while no increase of lipid peroxidation was detected in BALF (8-isoprostane). The absence of 8-OHdG following RE could be explained by lesions repairing systems induction after 24 h which would limit their later appearance and persistence over time. The main mechanism implied in these oxidative damages repair is base excision repair (Whitaker et al. 2017), but other intracellular actors such as p53 protein (Silva et al. 2014) or PARP-1 enzyme (Qin et al. 2008) may also contribute to damages repair. As previously shown, NPs inhalation could also initiate increased production of enzymes such as endonuclease III homolog 1 (NTH1) or apurinic/apyrimidinic endonuclease 1 (APE1) (Ma et al. 2013), p53 (Silva et al. 2014), or poly [ADP-ribose] polymerase 1 (PARP-1) (Qin et al. 2008), involved in various repair mechanisms and consequently limit side effects on nucleic acids. Lack of lipid peroxidation, assessed by 8-isoprostane dosing, in BALF might be due to the activation of the antioxidant response following exposures. Significant decreases of 8-isoprostane after RE to Al_2O_3 NPs or mixtures may also be due to changes of antioxidant balance. It would be interesting to perform glutathione peroxidase dosing in BALF in further studies to assess these antioxidant mechanisms (Romero et al. 1998). Moreover, reverse transcriptase polymerase chain reaction (RT-PCR) study of several antioxidant enzyme genes, such as superoxide dismutase 1 (SOD1), heme oxygenase-1 (Ho-1), or glutathione peroxidase1 (Gpx1), could also be performed to confirm this hypothesis (Constantino et al. 2014; Liu et al. 2017). In complement, western Blot analysis and

immunohistochemistry could be performed to assess other repairing mechanisms such as PARP-1, p53, APE1, and NTH1 (Qin et al. 2008; Ma et al. 2013; Silva et al. 2014).

As obtained results highlighted Al_2O_3 NPs lung retention 24 h after aerosols exposures, pro-inflammatory, and oxidative stress induction, the aerosols effect on alveolar–capillary barrier permeability was also studied. Significant elevations of LDH and total protein concentrations were measured in BALF only after RE to Al_2O_3 NPs and mixture aerosols containing HCl_g, indicating impairment of alveolar–capillary barrier permeability and cell cytolysis. These biological effects could be linked to pro-inflammatory mechanisms and PMN influx observed in lungs following RE to Al_2O_3 NPs alone or combined with HCl_g. Indeed, as previously demonstrated, PMN recruitment and pulmonary inflammation trigger alveolar–capillary barrier permeabilization (Williams and Chambers 2014; Wittekindt 2017). Alveolar–capillary barrier permeabilization could promote translocation of inhaled particles into bloodstream leading to potential systemic effects or local toxicity on other organs such as the brain, the liver, the spleen, or kidneys. A study is currently performed on these organs to assess local histopathological effects induced by aerosols inhalation.

Conclusion

In conclusion, inhalation exposure to Al_2O_3 NPs with or without HCl_g aerosols induce early pulmonary effects (24 h post-exposure) resulting in inflammation, oxidative stress, and alveolar–capillary barrier permeabilization. No synergistic or additive effect between Al_2O_3 NPs and HCl_g was observed on studied endpoints except for lung histopathology lesions nature (mainly vascular lesions observed with HCl_g, interstitial lesions observed with Al_2O_3 NPs and both observed after co-exposure). Obtained results underline that the exposure scenario mainly influences toxicological effects of mixtures. Al_2O_3 NPs presence in the aerosols also seems to play an essential role in driving toxicity (pro-inflammatory response, PMN, LDH and total protein increases, histopathological lesions and oxidative stress induction) compared to HCl_g (slight histopathological lesions and oxidative stress). Despite an increased pulmonary aluminum biodistribution in the case of RE to mixtures compared to Al_2O_3 NPs, similar pro-inflammatory responses were observed in the two conditions. SE induce oxidative stress resulting in nucleic oxidative damages, while RE essentially promote pulmonary inflammation. Special attention should be paid to pulmonary pro-inflammatory and oxidative stress induction as these phenomena are known to be closely linked to long-term pathologies such as pulmonary fibrosis or cancers (Reuter et al. 2010; Sesti et al. 2012; Khanna et al. 2014). Therefore, this pilot study raises concerns toward potential long-term pulmonary toxicity of combustion mixture aerosols. Further studies will have to be led to determine the potential toxicity of the mixture at longer times and lower doses. The latter information would then help to define dose limitations and exposure thresholds for workplace risk management. At the same time, better characterization of personnel exposure is still necessary, especially for military personnel who can be exposed due to operational constraints.

Ethics approval and consent to participate

In vivo experiments were approved by the "Comité Régional d'Ethique en Matière d'Expérimentation Animale" (CREMEAP) (C2EA-96).

Acknowledgments

The authors would like to thank the LASEM and Jean-Ulrich Mullot (LASEM, Toulon, FR) for aluminum ICP-OES dosing in lungs. They are indebted to Armel Descamps (UMS Castaing, Toulouse, FR) for TEM analyses and to Benjamin Duployer (CIRIMAT, Université de Toulouse, CNRS, Toulouse, FR) for Al_2O_3 NPs crystal structure determination. They acknowledge David Crouzier (IRBA, Brétigny-sur-Orge, FR) for his involvement in this project initiation. The authors also gratefully thank Marco Valente (IRBA, Brétigny-sur-Orge, FR), Claire Le Galliot (DGA, Paris, FR) and Noël Perrier (DGA, Paris, FR) for their reviewing and constructive feedback which helped to improve the manuscript.

Disclosure statement

The authors declare that they have no known competing financial interests or personal relationships that could have appeared to influence the work reported in this paper.

Funding

The French Government of Defense Procurement Agency, The Direction Générale de l'Armement (DGA), The Agence de l'Innovation Défense (AID), France, research program PROPERGOL funded this work.

ORCID

Emmanuel Flahaut http://orcid.org/0000-0001-8344-6902

References

Balasubramanyam A, Sailaja N, Mahboob M, Rahman MF, Hussain SM, Grover P. 2009. In vivo genotoxicity assessment of aluminium oxide nanomaterials in rat peripheral blood cells using the comet assay and micronucleus test. Mutagenesis. 24:245–251.

Barnes PJ. 2016. Inflammatory mechanisms in patients with chronic obstructive pulmonary disease. J Allergy Clin Immunol. 138(1): 16–27.

Biswas SK. 2016. Does the interdependence between oxidative stress and inflammation explain the antioxidant paradox? Oxid Med Cell Longev. 2016:5698931.

Carpizo DR, Reaka AJ, Glaws WR, Pooley N, Schmidt L, Halline AG, Goldstein JL, Layden TJ. 1998. Acute acid exposure increases rabbit esophageal cell proliferation. J Lab Clin Med. 131(2):157–162.

Chen L, Yokel RA, Hennig B, Toborek M. 2008. Manufactured aluminum oxide nanoparticles decrease expression of tight junction proteins in brain vasculature. J Neuroimmune Pharmacol. 3(4): 286–295.

Cheng L, Cao W, Behar J, Fiocchi C, Biancani P, Harnett KM. 2006. Acid-induced release of platelet-activating factor by human

esophageal mucosa induces inflammatory mediators in circular smooth muscle. J Pharmacol Exp Ther. 319(1):117–126.

Cheng L, Cao W, Fiocchi C, Behar J, Biancani P, Harnett KM. 2006. HCl-induced inflammatory mediators in cat esophageal mucosa and inflammatory mediators in esophageal circular muscle in an in vitro model of esophagitis. Am J Physiol Gastrointest Liver Physiol. 290(6):G1307–G1317.

Chivas-Joly C, Gaie-Levrel F, Motzkus C, Ducourtieux S, Delvallée A, De Lagos F, Nevé SL, Gutierrez J, Lopez-Cuesta J-M. 2016. Characterization of aerosols and fibers emitted from composite materials combustion. J Hazard Mater. 301:153–162.

Cho W-S, Duffin R, Thielbeer F, Bradley M, Megson IL, MacNee W, Poland CA, Tran CL, Donaldson K. 2012. Zeta potential and solubility to toxic ions as mechanisms of lung inflammation caused by metal/metal oxide nanoparticles. Toxicol Sci. 126(2):469–477.

Cohen MD. 2004. Pulmonary immunotoxicology of select metals: aluminum, arsenic, cadmium, chromium, copper, manganese, nickel, vanadium, and zinc. J Immunotoxicol. 1(1):39–69.

Constantino L, Goncalves RC, Giombelli VR, Tomasi CD, Vuolo F, Kist LW, de Oliveira GM, Pasquali MA, Bogo MR, Mauad T, et al. 2014. Regulation of lung oxidative damage by endogenous superoxide dismutase in sepsis. Intensive Care Med Exp. 2(1):17.

Darmer KI Jr, Kinkead ER, DiPasquale LC. 1974. Acute toxicity in rats and mice exposed to hydrogen chloride gas and aerosols. Am Ind Hyg Assoc J. 35(10):623–631.

Davis AS, Richter A, Becker S, Moyer JE, Sandouk A, Skinner J, Taubenberger JK. 2014. Characterizing and diminishing autofluorescence in formalin-fixed paraffin-embedded human respiratory tissue. J Histochem Cytochem. 62(6):405–423.

Dawe KER, Furlani TC, Kowal SF, Kahan TF, VandenBoer TC, Young CJ. 2019. Formation and emission of hydrogen chloride in indoor air. Indoor Air. 29(1):70–78.

Diggle JW, Downie TC, Goulding CW. 1970. The dissolution of porous oxide films on aluminium. Electrochim Acta. 15:1079–1093.

Dyer RF, Esch VH. 1976. Polyvinyl chloride toxicity in fires. Hydrogen chloride toxicity in fire fighters. JAMA. 235(4):393–397.

Franke MD, Ernst WR, Myerson AS. 1987. Kinetics of dissolution of alumina in acidic solution. Alche J. 33(2):267–273.

Galfetti L, Severini F, DeLuca L, Marra G, Meda L, Braglia R. 2004. Ballistics and condensed residues of aluminized solid rocket propellants. 9-IWCP "Novel Energetic Materials and Applications". Lerici, SP, Italy.

Hayes AW, Li R, Hoeng J, Iskandar A, Peistch MC, Dourson ML. 2019. New approaches to risk assessment of chemical mixtures. Toxicol Res Appl. 3(6):239784731882076

Huang S, Paulauskis JD, Godleski JJ, Kobzik L. 1992. Expression of macrophage inflammatory protein-2 and KC mRNA in pulmonary inflammation. Am J Pathol. 141(4):981–988.

Kaplan HL, Anzueto A, Switzer WG, Hinderer RK. 1988. Effects of hydrogen chloride on respiratory response and pulmonary function of the baboon. J Toxicol Environ Health. 23(4):473–493.

Kellum JA, Song M, Li J. 2004. Lactic and hydrochloric acids induce different patterns of inflammatory response in LPS-stimulated RAW 264.7 cells. Am J Physiol Regul Integr Comp Physiol. 286(4): R686–R692.

Khanna H, Karki K, Pande D, Negi R, Khanna R. 2014. Inflammation, free radical damage, oxidative stress and cancer. Interdiscip J Microinflammation. 1(1):109.

Khanna P, Ong C, Bay BH, Baeg GH. 2015. Nanotoxicity: an interplay of oxidative stress, inflammation and cell death. Nanomaterials (Basel). 5(3):1163–1180.

Kim YS, Chung YH, Seo DS, Choi HS, Lim CH. 2018. Twenty-eight-day repeated inhalation toxicity study of aluminum oxide nanoparticles in male Sprague–Dawley rats. Toxicol Res. 34(4):343–354.

Kongerud J, Soyseth V. 2014. Respiratory disorders in aluminum smelter workers. J Occup Environ Med. 56(5 Suppl):S60–S70.

Krewski D, Yokel RA, Nieboer E, Borchelt D, Cohen J, Harry J, Kacew S, Lindsay J, Mahfouz AM, Rondeau V. 2007. Human health risk assessment for aluminium, aluminium oxide, and aluminium hydroxide. J Toxicol Environ Health B Crit Rev. 10(Suppl 1):1–269.

Kwon JT, Seo GB, Lee MJ, Kim HM, Shim I, Jo E, Kim P, Choi K. 2013. Pulmonary toxicity assessment of aluminum oxide nanoparticles via nasal instillation exposure. J Environ Health Sci. 39:48–55.

Lamkanfi M, Dixit VM. 2014. Mechanisms and functions of inflammasomes. Cell. 157(5):1013–1022.

Li X, Yang H, Wu S, Meng Q, Sun H, Lu R, Cui J, Zheng Y, Chen W, Zhang R, et al. 2017. Suppression of PTPN6 exacerbates aluminum oxide nanoparticle-induced COPD-like lesions in mice through activation of STAT pathway. Part Fibre Toxicol. 14(1):53.

Lippmann M, Yeates DB, Albert RE. 1980. Deposition, retention, and clearance of inhaled particles. Br J Ind Med. 37(4):337–362.

Liu Y, Lu F, Kang L, Wang Z, Wang Y. 2017. Pirfenidone attenuates bleomycin-induced pulmonary fibrosis in mice by regulating Nrf2/Bach1 equilibrium. BMC Pulm Med. 17(1):63.

Liu T, Zhang L, Joo D, Sun SC. 2017. NF-kappaB signaling in inflammation. Signal Transduct Target Ther. 2: 17023.

Lugrin J, Rosenblatt-Velin N, Parapanov R, Liaudet L. 2014. The role of oxidative stress during inflammatory processes. Biol Chem. 395(2):203–230.

Ma J, Altomare A, de la Monte S, Tong M, Rieder F, Fiocchi C, Behar J, Shindou H, Biancani P, Harnett KM. 2010. HCl-induced inflammatory mediators in esophageal mucosa increase migration and production of H2O2 by peripheral blood leukocytes. Am J Physiol Gastrointest Liver Physiol. 299:G791–G798.

Machle W, Kitzmiller KV, Scott EW, Treon JF. 1942. The effect of the inhalation of hydrogen chloride. J Ind Hyg Toxicol. 24:222–225.

Ma H, Wang J, Abdel-Rahman SZ, Boor PJ, Khan MF. 2013. Induction of base excision repair enzymes NTH1 and APE1 in rat spleen following aniline exposure. Toxicol Appl Pharmacol. 267(3): 276–283.

Meda L, Marra G, Galfetti L, Inchingalo S, Severini F, Deluca L. 2005. Nano-composites for rocket solid propellants. Compos Sci Technol. 65:769–773.

OECD/OCDE403. 2009a. Guidelines for the Testing of Chemicals – Acute Inhalation Toxicity. 403. OECD/OCDE.

OECD/OCDE412. 2009b. Guidelines for the Testing of Chemicals – Subacute Inhalation Toxicity: 28-Day Study. 412. OECD/OCDE.

OECD/OCDE436. 2009c. Guidelines for the Testing of Chemicals – Acute Inhalation Toxicity – Acute Toxic Class Method. 436. OECD/OCDE.

Parasuraman S. 2011. Toxicological screening. J Pharmacol Pharmacother. 2(2):74–79.

Paur H-R, Cassee FR, Teeguarden JG, Fissan HJ, Diabate S, Aufderheide M, Kreyling WG, Hänninen O, Kasper G, Riediker M, et al. 2011. In-vitro cell exposure studies for the assessment of nanoparticle toxicity in the lung—A dialog between aerosol science and biology. J Aerosol Sci. 42(10):668–692.

Pellett GL, Sebacher DI, Bendura RJ, Wornom DE. 1983. HCI in rocket exhaust clouds: atmospheric dispersion, acid aerosol characteristics, and acid rain deposition. J Air Pollut Control Assoc. 33: 304–311.

Pichard A, Bisson M, Gay G, Houeix N, Jolibois B, Lefevre JP, Magaud H, Migné V, Morin A, Tissot S. 2005. Fiche de données toxicologiques et environnementales des substances chimiques: Aluminium et Dérivés – INERIS.

Pirela SV, Bhattacharya K, Wang Y, Zhang Y, Wanga G, Christophi CA, Godleski J, Thomas T, Qiane Y, Orandlee MS, et al. 2019. A 21-day sub-acute, whole-body inhalation exposure to printer-emitted engineered nanoparticles in rats: Exploring pulmonary and systemic effects. NanoImpact. 15:100176.

Piriyawong V, Thongpool V, Asanithi P, Limsuwan P. 2012. Preparation and characterization of alumina nanoparticles in deionized water using laser ablation technique. J Nanomater. 2012:1–6.

Prabhakar PV, Reddy UA, Singh SP, Balasubramanyam A, Rahman MF, Indu Kumari S, Agawane SB, Murty US, Grover P, Mahboob M. 2012. Oxidative stress induced by aluminum oxide nanomaterials after acute oral treatment in Wistar rats. J Appl Toxicol. 32(6): 436–445.

Pritchard JN. 1989. Dust overloading causes impairment of pulmonary clearance: evidence from rats and humans. Exp Pathol. 37(1–4): 39–42.

Qin XJ, Hudson LG, Liu W, Ding W, Cooper KL, Liu KJ. 2008. Dual actions involved in arsenite-induced oxidative DNA damage. Chem Res Toxicol. 21(9):1806–1813.

Reuter S, Gupta SC, Chaturvedi MM, Aggarwal BB. 2010. Oxidative stress, inflammation, and cancer: how are they linked? Free Radic Biol Med. 49(11):1603–1616.

Romero FJ, Bosch-Morell F, Romero MJ, Jareno EJ, Romero B, Marin N, Roma J. 1998. Lipid peroxidation products and antioxidants in human disease. Environ Health Perspect. 106(Suppl 5):1229–1234.

Salzano S, Checconi P, Hanschmann EM, Lillig CH, Bowler LD, Chan P, Vaudry D, Mengozzi M, Coppo L, Sacre S, et al. 2014. Linkage of inflammation and oxidative stress via release of glutathionylated peroxiredoxin-2, which acts as a danger signal. Proc Natl Acad Sci U S A. 111(33):12157–12162.

Saperstein S, Huyck H, Kimball E, Johnston C, Finkelstein J, Pryhuber G. 2009. The effects of interleukin-1beta in tumor necrosis factor-alpha-induced acute pulmonary inflammation in mice. Mediators Inflamm. 2009:958658.

Schlesinger RB, Snyder CA, Chen LC, Gorczynski JE, Menache M. 2000. Clearance and translocation of aluminum oxide (alumina) from the lungs. Inhal Toxicol. 12(10):927–939.

Sellakumar AR, Snyder CA, Solomon JJ, Albert RE. 1985. Carcinogenicity of formaldehyde and hydrogen chloride in rats. Toxicol Appl Pharmacol. 81:401–406.

Sesti F, Tsitsilonis OE, Kotsinas A, Trougakos IP. 2012. Oxidative stress-mediated biomolecular damage and inflammation in tumorigenesis. In Vivo. 26(3):395–402.

Sgro LA, D'Anna A, Minutolo P. 2012. On the characterization of nanoparticles emitted from combustion sources related to understanding their effects on health and climate. J Hazard Mater. 211–212:420–426.

Sikkeland L, Alexis NE, Fry RC, Martin E, Danielsen TE, Sostrand P, Kongerud J. 2016. Inflammation in induced sputum after aluminium oxide exposure: an experimental chamber study. Occup Environ Med. 73(3):199–205.

Silva AR, Santos AC, Farfel JM, Grinberg LT, Ferretti RE, Campos AH, Cunha IW, Begnami MD, Rocha RM, Carraro DM, et al. 2014. Repair of oxidative DNA damage, cell-cycle regulation and neuronal death may influence the clinical manifestation of Alzheimer's disease. PLoS One. 9(6):e99897.

Simon-Vazquez R, Lozano-Fernandez T, Davila-Grana A, Gonzalez-Fernandez A. 2016. Analysis of the activation routes induced by different metal oxide nanoparticles on human lung epithelial cells. Future Sci OA. 2(2)FSO:118.

Sliwinska A, Kwiatkowski D, Czarny P, Milczarek J, Toma M, Korycinska A, Szemraj J, Sliwinski T. 2015. Genotoxicity and cytotoxicity of ZnO and Al2O3 nanoparticles. Toxicol Mech Methods. 25:176–183.

Stavert DM, Archuleta DC, Behr MJ, Lehnert BE. 1991. Relative acute toxicities of hydrogen fluoride, hydrogen chloride, and hydrogen bromide in nose- and pseudo-mouth-breathing rats. Fundam Appl Toxicol. 16(4):636–655.

Tanino Y, Coombe DR, Gill SE, Kett WC, Kajikawa O, Proudfoot AE, Wells TN, Parks WC, Wight TN, Martin TR, et al. 2010. Kinetics of chemokine-glycosaminoglycan interactions control neutrophil migration into the airspaces of the lungs. J Immunol. 184(5): 2677–2685.

Toews GB. 2001. Cytokines and the lung. Eur Respir J Suppl. 34: 3s–17s.

Tornling G, Blaschke E, Eklund A. 1993. Long term effects of alumina on components of bronchoalveolar lavage fluid from rats. Br J Ind Med. 50(2):172–175.

Wang K-S, Chiang K-Y, Lin S-M, Tsai C-C, Sun C-J. 1999. Effects of chlorides on emissions of hydrogen chloride formation in waste incineration. Chemosphere. 38:1571–1582.

Whitaker AM, Schaich MA, Smith MR, Flynn TS, Freudenthal BD. 2017. Base excision repair of oxidative DNA damage: from mechanism to disease. Front Biosci (Landmark Ed). 22:1493–1522.

Williams AE, Chambers RC. 2014. The mercurial nature of neutrophils: still an enigma in ARDS? Am J Physiol Lung Cell Mol Physiol. 306(3):L217–L230.

Wittekindt OH. 2017. Tight junctions in pulmonary epithelia during lung inflammation. Pflugers Arch. 469(1):135–147.

Wohlslagel J, Dipasquale LC, Vernot EH. 1976. Toxicity of solid rocket motor exhaust: effects of HC1, HF and alumina on rodents. J Combustion Toxicol. 3:61–70.

Yin K, Hock CE, Lai PS, Ross JT, Yue G. 1999. Role of interferon-gamma in lung inflammation following cecal ligation and puncture in rats. Shock. 12(3):215–221.

Zhang Q, Wang H, Ge C, Duncan J, He K, Adeosun SO, Xi H, Peng H, Niu Q. 2017. Alumina at 50 and 13 nm nanoparticle sizes have potential genotoxicity. J Appl Toxicol. 37(9):1053–1064.

Zhu YZ, Liu DW, Liu ZY, Li YF. 2013. impact of aluminum exposure on the immune system: a mini review. Environ Toxicol Pharmacol. 35(1):82–87.